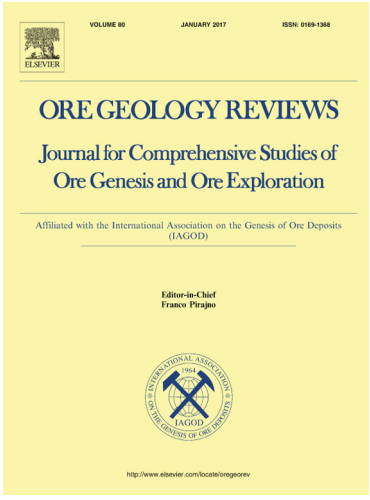

Precious metals assemblages at the Mikheevskoe porphyry copper deposit (South Urals, Russia) as proxies of epithermal overprinting

Olga.Y. Plotinskaya, Oksana B. Azovskova, Sergei S. Abramov, Elena O. Groznova, Konstantin A. Novoselov, Reimar Seltmann, John Spratt

PII: S0169-1368(17)30702-3
DOI: https://doi.org/10.1016/j.oregeorev.2018.01.025
Reference: OREGEO 2470

To appear in: *Ore Geology Reviews*

Received Date: 15 September 2017
Revised Date: 5 January 2018
Accepted Date: 21 January 2018

Please cite this article as: Olga.Y. Plotinskaya, O.B. Azovskova, S.S. Abramov, E.O. Groznova, K.A. Novoselov, R. Seltmann, J. Spratt, Precious metals assemblages at the Mikheevskoe porphyry copper deposit (South Urals, Russia) as proxies of epithermal overprinting, *Ore Geology Reviews* (2018), doi: https://doi.org/10.1016/j.oregeorev.2018.01.025

Precious metals assemblages at the Mikheevskoe porphyry copper deposit (South Urals, Russia) as proxies of epithermal overprinting

Olga. Y. Plotinskaya [a], Oksana B. Azovskova [b], Sergei S. Abramov [a], Elena O. Groznova [a,c], Konstantin A. Novoselov [d], Reimar Seltmann [e], John Spratt [e]

[a] Institute of Geology of Ore Deposits, Petrography, Mineralogy and Geochemistry, Russian Academy of Sciences (IGEM RAS), Staromonetny per. 35, Moscow 119017, Russia

[b] The Zavaritsky Institute of Geology and Geochemistry, Ural Branch of Russian Academy of Sciences, Akademika Vonsovskogo str. 15, Yekaterinburg 620016, Russia

[c] Institute of Experimental Mineralogy, Russian Academy of Sciences (IEM RAS), Chernogolovka, Moscow oblast', 142432, Russia

[d] Institute of Mineralogy, Ural Branch of Russian Academy of Sciences, 456317 Miass, Chelyabinsk oblast, Russia

[e] Natural History Museum, London SW7 5BD, UK

Abstract

Mineral assemblages and formation conditions of precious metals (Au, Ag, PGE) in ores of the Mikheevskoe porphyry copper deposit (South Urals) are the subject of our study. Three mineralization types can be distinguished: (1) Gold-silver-telluride mineralization overlapping porphyry-style bornite-chalcopyrite ores includes native gold (fineness 863-873), electrum (fineness 593-672), galena, hessite, coloradoite, and, more rarely, petzite, stützite, Au-Ag ditellurides, native tellurium, tellurobismuthite, tetradymite–kawazulite, altaite, and extremely rare melonite $NiTe_2$, merenskyite $PdTe_2$, and sopcheite $Ag_4Pd_3Te_4$; (2) Gold-arsenopyrite-base-metal mineralization within quartz-tetrahedrite-sphalerite veinlets cutting porphyry-style mineralization; (3) Gold-telluride mineralization with argillic alteration and mineralogically similar to that of type (1) but distinct because of the presence of Au-Ag, Ag, and Pb selenides. Textural relationships supported by fluid inclusions data and chlorite geothermometry provide evidence that occurrence of precious metals minerals at the Mikheevskoe deposit is mostly linked to epithermal overprint of the porphyry mineralization and was deposited at ca. 300 to 200^{o}C from moderately saline fluids (ca. 5 to 10 wt.%-eq.NaCl). It is suggested that the observed variability in Au and Ag minerals results from small fluctuations of S_2 and/or Te_2 fugacity.

1 Introduction

Gold and silver are important by-products in porphyry Cu(-Mo) deposits and despite their low concentrations (tenths ppm), ca. 20% of global gold production comes from porphyry deposits (Sillitoe, 2010). The deposits of the Almalyk group in Uzbekistan (Kalmakyr, Dalnee, etc.) contain over 2,000 t Au, and the Oyu Tolgoi group (Mongolia) contains over 1,400 t Au (Seltmann et al., 2014). Platinum group elements (PGE) are also present but at much lower concentrations: Pd contents reach hundreds ppb in sulfide or flotation concentrates at some deposits and several ppm in selected samples (Tarkian and Stribrny, 1999; Economou-Eliopoulos, 2005; Eliopoulos et al., 2014; Economou-Eliopoulos et al., 2017; Sotnikov et al., 2001; Berzina and Korobeinikov, 2007). For example, Pasava et al. (2010) estimated approximately 17 t of Pd and 1.7 t of Pt in the Kalmakyr deposit.

It is widely known that during the life-cycle of a porphyry system native gold can be deposited at least twice (Kesler et al., 2002; Sillitoe, 2010). The early native gold associates with bornite-chalcopyrite assemblages. Later Au and Ag mineralization is related to epithermal overprint which is featured by a more diverse mineralogy, and, even more important, establish distribution patterns and structural control different from disseminated porphyry-style mineralization (Kesler et al., 2002). This makes a study of mineralogy, distribution patterns, and formation conditions of precious metals (Au, Ag, and PGE) in porphyry deposits important from both academic and economical points of view.

This paper is focused on the Mikheevskoe deposit, the largest porphyry copper deposit in the Urals (Volchkov et al., 2015), and aims to describe mineral forms of precious metals, their mineral assemblages as well as to evaluate conditions of their deposition.

The Russian Copper Company started an open-pit mining of the Mikheevskoe deposit in 2013 (Russian Copper Company). The estimated reserves (Russian categories A+B+C) of the deposit as of September 20th, 2017 are 629 Mt of ore at 0.41% Cu (Russian Copper Company; Vestnik…, 2017) which makes ca. 2.6 Mt of contained Cu. Earlier Volchkov et al. (2015) reported 347 Mt of ore at 0.45% Cu and 0.137 ppm Au with 46.9 t of contained Au. PGE reserves were not estimated, but Grabezhev et al. (2013) reported Pt (4 to 37 ppb) and Pd (2 to 98 ppb) in six pyrite and chalcopyrite mineral concentrates.

2 Geological background

The Mikheevskoe deposit is located in the South Urals approximately 200 km south of Chelyabinsk city (Fig. 1, inset). The deposit is part of the Novonikolaevsk ore cluster, which is confined to a ca. 20 km wide north-trending volcanic terrane at the junction of the East- and Transuralian terranes (or megazones), both of which are considered most prospective for porphyry-style mineralization in the Urals (Plotinskaya et al., 2017; Hammarstrom et al., 2017). Volcanic sequences of the Transuralian, as well as dioritic porphyry intrusions and related porphyry copper and skarn mineralization, are linked to a subduction event which lasted from the Late Devonian to the Early Carboniferous (Samygin and Burtman, 2009; Puchkov, 2017 and references therein).

The Mikheevskoe deposit is hosted by a Late Devonian to Early Carboniferous (Tournaisian) volcano-sedimentary sequence comprising two lithological units (Belgorodskii et al., 1991). The lower unit consists of interbedded sandstone, tuffaceous sandstone, basaltic andesite, and tuffaceous breccia with subordinate siltstone, carbonaceous−cherty rocks, and basalt. The upper unit comprises of aphyric basaltic lava and pyroclastics with intercalated sandstone, quartzite, and carbonaceous–cherty rocks with numerous serpentinite bodies (Fig. 1).

The intrusive rocks belong to Late Devonian to Early Carboniferous Ulyanovsk and Mikheevsky calk-alkaline igneous complexes (Grabezhev and Belgorodskii, 1992; Grabezhev, 2014). Intrusions of the earlier *Ulyanovsk Complex* are stocks and dikes of porphyritic diorite and andesite, and less frequent dacite, rhyodacite, and dolerite of the low-K series. Intrusions of the later *Mikheevsky Complex*, which are supposed to be linked to porphyry Cu mineralization (Belgorodskii et al., 1991), belong to the moderate-K series. These comprise equigranular and porphyritic rocks forming porphyry stocks and dykes, among which diorite, diorite porphyry, and plagiogranodiorite porphyry are the most common (Figs. 1 and 2a) (Grabezhev and Belgorodskii, 1992; Grabezhev, 2014). Post-ore dykes of plagiogranodiorite porphyry are also ascribed to the Mikheevsky complex (Grabezhev, 2014). Diorite porphyry of the Mikheevsky Complex was dated as 356 ± 6 Ma (U-Pb SHRIMP zircon age; Grabezhev and Ronkin, 2011), which is in good agreement with the Re-Os age of molybdenite (357.8 ± 1.8 Ma and 356.1 ± 1.4 Ma) obtained by Tessalina and Plotinskaya (2017). Porphyry-style mineralization is confined to a swarm of dykes of diorite, plagiogranodiorite and their porphyry equivalents of the Mikheevsky complex, covering an area of ca. 0.5 × 3 km that trends approximately north-south in between two large diorite stocks (Figs. 1 and 2).

Plotinskaya et al. (2015) proposed the following sequence of main alteration types for the deposit. The *sodic–calcic alteration,* found in the central zone of the deposit, is composed of an actinolite ± epidote assemblage; it accompanies rare magnetite mineralization. *Potassic alteration* is common in the central part of the deposit. Altered rocks composed of biotite + muscovite ± K-feldspar accompany bornite–chalcopyrite mineralization. *Phyllic alteration* (quartz–sericite) accompany molybdenite–chalcopyrite mineralization. *Propylites* (chlorite + epidote + sericite) are abundant on the margins of the deposit. The most abundant *chlorite–sericite* altered rocks form transitional zones between phyllic and propylitic alteration. *Argillic alteration* occurs as several steeply dipping zones of intense clay-altered rocks with rare disseminated pyrite. The *oxidation zone,* approximately 15 m thick, is composed of clays with residual quartz, malachite and azurite (Belgorodskii et al., 1991).

3 Methods

The bulk mineral composition of altered rocks was estimated using Shimadzu XRD-7000 X-ray diffractometer and PerkinElmer Diamond TG/DTA system in the Zavaritsky Institute of Geology and Geochemistry, Ural Branch, Russian Academy of Sciences (IGG UB RAS), Yekaterinburg, analysts: N.G. Petrishcheva and T.Ya. Gulyaeva.

3.1 Scanning electron microscopy (SEM) and electron probe micro analysis (EPMA) study

The chemical compositions of ore and gangue minerals were determined using SEM with Energy Dispersive X-ray (EDX) detectors: Tescan Vega TS 5130 MM (SEM) with Oxford Instruments INCAPenta FETx3 (EDX) detector and Tescan Vega II XMU (SEM) with Oxford Instruments INCA xSight (EDX) detector (Institute of Experimental Mineralogy, Russian Academy of Sciences, Chernogolovka, analyst: A.N. Nekrasov), Tescan Vega 3 SBU (SEM) with Oxford Instruments X-act (EDX) detector (Institute of Mineralogy, the Urals Branch of Russian Academy of Sciences (IMin UB RAS), Miass, analyst: I.A. Blinov), Jeol JSM-6390LV (SEM) with Oxford Instruments X-Max 80 (EDX) detector (IGG UB RAS), Yekaterinburg, analyst: S.P. Glavatskikh), and Zeiss EVO 15LS (SEM) with Oxford Instruments X-Max (EDX) detector (Natural History Museum, London, UK). Cathodoluminescence (CL) images were additionally obtained with the Zeiss EVO 15LS (SEM), Natural History Museum, London, UK.

Selected grains of native gold and minerals of fahlore group were analyzed using a JEOL JXA-8200 (EPMA) with five wavelength dispersive X-ray (WDX) detectors (Institute of Geology of Ore Deposits, Petrography, Mineralogy, and Geochemistry, Russian Academy of Sciences (IGEM RAS), analyst I.G. Griboedova) and the following operating conditions were used: accelerating

voltage 20 kV, sample current – 20 nA; beam diameter 1-2 μm; exposition time 10 to 20 sec.; detection limits (1σ) 0.01 to 0.05 wt.%. For *native gold* the following X-ray lines were used: L_α for Au, Ag, and Te, K_α for Cu and M_β for Hg; standards: HgS for Hg and pure metals for remaining elements. For *fahlore group* the following X-ray lines were used: K_α for S, Cu, Fe, and Zn, L_α for Sb, Se, Ag, As, Te, L_β for Cd, M_α for Pb and Bi; standards CdSe for Se and Cd, Sb_2S_3 for S and Sb, $CuFeS_2$ for Fe, GaAs for As, HgS for Hg, PbS for Pb, ZnS for Zn, $AgSbS_2$ for Ag, and pure metals for Cu, Te, and Bi.

3.2 Fluid inclusion study

Microthermometric measurements were carried out using a THMSG-600 (Linkam) microscope heating-freezing stage at the Institute of Experimental Mineralogy of Russian Academy of Sciences (IEM RAS), Chernogolovka. The temperature of phase transitions were measured within the range –196 to +600°C with an accuracy of ±0.2°C within the interval +20 to –20°C and no less than ±1.0°C beyond this interval. The salt composition of the fluids was determined from the eutectic temperature (T_e) according to Crawford (1981); the salinity was estimated from the temperature of ice melting (T_m) using the NaCl–H_2O phase diagram (Bodnar and Vityk, 1994). The measurements were carried out for clusters of inclusions with similar phase relationships to avoid errors related to the disintegration of vacuoles after fluid heterogenization (Roeder, 1984).

4 Mineralogy of precious metals

Gold, silver, and especially PGE minerals are extremely rare at the Mikheevskoe deposit. With few exceptions, they were found in the central part of the northern segment of the deposit (Fig. 1). According to Shargorodskii et al. (2005), this segment, which strikes north-south for over 850 m, is the most economically significant. The richest ore is confined to the central zone of the northern segment (Fig. 2b) forming an ore-shoot with ca. 200kt of Cu at 0.9-1.0% (Shargorodskii et al., 2005). We identified three groups of precious metal assemblages: (1) gold-silver-telluride in bornite-chalcopyrite veinlet-disseminated mineralization, (2) gold-arsenopyrite-base-metal and (3) gold-silver-telluride related to argillic alteration.

4.1 Gold-silver-telluride mineralization

Gold-silver-telluride mineralization was found exclusively in the Northern segment of the deposit and mostly within the richest ore with >1% Cu (Fig. 2b). Ore is composed of chalcopyrite and, to a lesser degree, bornite and molybdenite within biotite alteration envelope developed after andesite-basalt volcanoclastics. Biotite, however, is extensively replaced by sericite (Fig. 3a), quartz-sericite (Fig. 3b), or chlorite-epidote (Fig. 3c) assemblages. Mineralization of gold-silver-

telluride type includes native gold and a variety of tellurides (Tables 1 and 2) forming inclusions in bornite, chalcopyrite, chalcocite, rarely in molybdenite, minerals of cobaltite-gersdorffite series, epidote, and chlorite. Such inclusions rarely exceed several microns in size, making identification challenging; nevertheless, over a dozen minerals forming several assemblages were identified.

In the *gold-telluride assemblage, native gold* occurs as isometric, rounded or oval, sometimes amoeba-like inclusions in bornite, 1 to 20 microns in size. In most cases gold inclusions are confined to marginal zones of bornite grains (Fig. 3d-h). Gold is intergrown with galena (Fig. 3d), *petzite* Ag_3AuTe_2 (Fig. 3e,f), as well as with minerals too small to be identified, presumably Au-Ag ditelluride (*krennerite* $(AuAg)Te_2$?) and Bi sulfide (Fig. 3g,h). A micron-scale grain of native gold was found on the boundary of chalcopyrite and cobaltite-gersdorffite (from $(Co_{0.8},Ni_{0.1},Fe_{0.1})_{\Sigma 1}AsS$ to $(Co_{0.5},Ni_{0.5})_{\Sigma 1}AsS$) in assemblage with *melonite* $NiTe_2$ and *altaite* PbTe (Fig. 3i-k).

Native gold varies widely in chemical composition (Table 1). In assemblage with galena, it contains 12.4 to 13.5 wt.% Ag and ca. 1.5 wt.% Cu, for the latter, however, Cu was likely captured from hosting bornite (Table 1, analysis 1 and 2). In electrum, associated with petzite, the Ag content is 37.4 to 40.6 wt.%, while with krennerite (?), it is 33 wt.% (Table 1, analysis 3 to 5).

Silver tellurides occur in bornite and, similar to the gold-telluride assemblage described above, they tend to be confined to grain margins or to boundaries of bornite and chalcopyrite grains. Silver tellurides are *hessite* (Ag_2Te) and *stützite* ($Ag_{5-x}Te_3$), but in many cases it is impossible to distinguish due to the small sizes (Fig. 4).

Silver tellurides are associated with native tellurium and with bismuth sulfotellurides (Fig. 4, a-c) and, sometimes, with altaite and *coloradoite* HgTe (Fig. 4d) or form intergrowths with *tetradymite* $(Bi_2Te_2(S_{0.8}Se_{0.1})_{0.9})$, *kawazulite* $(Bi_2Te_2(Se_{0.6}S_{0.3})_{0.9})$, and coloradoite on the boundary of chalcopyrite and quartz (Fig. 4, e-f). Coloradoite also often forms oval inclusions in bornite or anhedral grains in epidote and chlorite overgrowing bornite or chalcopyrite. In addition, silver tellurides occur as micron-scale inclusions between molybdenite flakes (Fig. 5).

Assemblage of *hessite with palladium tellurides* was observed only in one sample (M-1/139) in chalcopyrite (Fig. 6). *Merenskyite* ($PdTe_2$) occurs as oval micron-scale grains intergrown with hessite and coloradoite (Fig. 6a). The largest grain (ca. 2x3 μm) contains notable admixtures of Ni (0.9 wt.%). The only grain of *sopcheite* ($Ag_4Pd_3Te_4$), also 2x3 μm in size, was found in intergrowth with merenskyite and hessite (Fig. 6b,c).

In one sample (M-5/17), mineralization of gold-silver-telluride type was found in bornite-chalcocite association (Fig.7), which is represented by large nests of bornite in white quartz veins (Fig. 7a). Chalcocite overgrows bornite and also forms myrmekitic inclusions in it (Fig.7b,c) while

192 calcite and fahlore (intermediate tenanntite-tetrahedrite member) overgrow both chalcocite and
193 bornite (Fig.7c). Hessite forms micron-scale inclusions confined to boundaries of bornite and
194 quartz (Fig.7d) or bornite and chalcocite (Fig.7e). In bornite hessite inclusions often form “chains”,
195 presumably tracing fractures (Fig.7c). Hessite often associates with galena (Fig. 7d,e) which
196 contains tenths wt.% of Se (Table 2). Electrum was observed exclusively in bornite as worm-like
197 micron-scale inclusions (Fig. 7f). The Ag content varies from 33.4 to 40.6 wt.%, Hg is also present in
198 small amounts (Table 1, analysis 7 to 9).

199 **4.2 Gold-arsenopyrite-base metal mineralization**

200 Mineralization of this type occurs within milky-white quartz veins from several cm to tens
201 cm thick (Fig. 8a), both in central (samples M9/15 and M6/16) and marginal zones (samples M-
202 3/16 and M-48/138.7) of the deposit (Figs 1 and 2b). The veins contain clusters of pyrite,
203 arsenopyrite, chalcopyrite, fahlore, galena, and sphalerite (Fig. 8b-g).

204 Electrum forms micron-scale stringers in arsenopyrite near its contacts with sphalerite (Fig.
205 8b) or fahlore (Fig. 8g-i). Silver contents in electrum associated with fahlore make up 11 to
206 28.4 wt.% (Table 1, analysis 10-13), while electrum intergrown with galena and sphalerite contain
207 44.5 to 25.7 wt.% of Ag and up to 4 wt.% of Hg (Table 1, analysis 14-16).

208 Minerals of fahlore group in this type of mineralization vary from an intermediate
209 tennantite-tetrahedrite to tetrahedrite end-member with an almost equal Fe to Zn ratio and low,
210 up to 0.7 wt.%, Ag content (Table 3, analysis 1 to 3). In some cases, small grains of fahlore varying
211 in composition from argentoan tetrahedrite (3.6 to 24.4 wt.% of Ag) to freibergite (33.0 wt.% of
212 Ag) in assemblage with polybasite overgrow chalcopyrite and sphalerite (Fig. 8d).

213 In the marginal zone of the southern segment of the deposit, white quartz-calcite veinlets
214 in propylitized basalt contain visible native gold, up to 1-2 mm in size (Fig. 8j, sample 7905/190.6).
215 In a polished section, gold forms veinlets up to 0.3mm thick, which overgrow and cement
216 chalcopyrite and pyrite, and is intergrown with clay mineral, presumably kaolinite or dickite (Fig.
217 8k-i). The largest gold grains contain 11.5 to 13 wt.% of Ag and up to 0.3 wt.% of Hg (Table 1,
218 analysis 17-27), while smaller isometric gold grains of 5 to 10 μm in size are confined to calcite;
219 they have 8.4 – 9 wt.% of Ag while Hg is below detection limit (0.04 wt.%). This sample is also
220 referred to the gold-arsenopyrite-base-metal type mineralization because of similarity in gold
221 composition.

4.3 Precious metals mineralization in argillic alteration

Two zones of argillic alteration, exposed in the open-pit, located 400 m apart, were studied. Both zones, 20 to 25 m thick, are composed of intense clay altered rocks of white, light-gray, with greenish or yellow shade, occasionally with silicified zones. The first one (Arg-1) is located in the Northern part of the open pit (samples Mikh-7, Mikh-14-1, Mikh-T-1), the second one (Arg-2) is in the central part of the open pit (samples Mikh-11-1, Mikh-15-1, Mikh-15-2, Mikh-T-2, Mikh-T-3). Thermal and X-ray data show argillaceous rocks, consisting of mainly quartz, illite/hydromica, sulfides (1 to 5 %), in some cases chlorite, carbonates (calcite, dolomite, and siderite), kaolinite and carbonaceous matter (low-temperature bitumen) (Azovskova et al., 2015). Pyrite, chalcopyrite, copper sulfides, molybdenite are major ore minerals (in order of listing); cobalt and nickel sulfoarsenides are also present.

Minerals of precious metals in argillic altered rocks were observed only overgrowing pyrite grains (Figs. 9 and 10), along with inclusions of chalcopyrite, molybdenite, galena, sphalerite, arsenopyrite, cobaltite, gersdorffite, alloclasite (Figs. 9b,d, 10e); occasionally tennantite and unidentified Bi- and Pb-Bi- sulfosalts and Cu sulfides. Tellurides are also common and include hessite, which is the most wide-spread (Figs. 9d,f,I, 10f), coloradoite, altaite, tellurobismuthite, unidentified telluride of Au-Ag. Naumannite (Ag_2Se) is the only selenide found (Fig 9c), but mixtures of Au-Ag-Se, Cu-Ag-Se, and Ag-Pb-Se-(± Bi) phases were also observed (Fig. 9c,d,f,g,h).

Native gold occurs as small grains (up to 10 μm) and is variable in chemical composition (fineness from 1000 to 306-360), electrum with lowest fineness sometimes contains up to 10 wt.% of Hg (Figs.9b, 10a-e, Table 1, analyses 28–23). This compositional variation is much wider than one observed for mineralization of gold-silver-telluride type, but it is similar to one reported for mineralization of gold-arsenopyrite-base-metal type (Fig. 11).

5 Chemistry of associated minerals

5.1 White mica chemistry

Sericite is present in alteration haloes of all investigated samples with Au-Ag mineralization. However in most cases, it occurs as micron-scale disseminated grains in intimate intergrowths with other minerals (biotite, albite, chlorite, carbonate, etc.). Relatively large sericite accumulations were observed and analyzed only in four samples, namely M-52/67.1, M-5/17, M-7905/190.6, and M-3/16. In the sample M-52/67.1 white mica is associated with chlorite, pumpellyite, epidote, titanite, etc. (Fig. 3i). It is represented by muscovite-phengite series (Mg+Fe 0.2 to 0.4 apfu) with a clearly pronounced isomorphic substitution FeMg+Si<–>Al (Fig. 12a). In the

sample M-3/16, sericite, associating with ankerite-dolomite, quartz, minor albite, as well as with galena, and sphalerite, belongs to muscovite-paragonite series (X(Na) from 0.1 to 0.8). In the sample M-5/17, white mica intergrown with bornite and chalcocite has low (K+Na) contents (0.6 to 0.7 apfu) at elevated X(Na)=0.2 to 0.3 and high Si content (3.4 to 3.5 apfu) and, thus belongs to illite with minor amount of a paragonite end-member (Table 4, Fig. 12b). Similar mica was reported earlier by Grabezhev and Bakhtina (1991) within rare chlorite-carbonate-muscovite-paragonite-quartz alteration zones. The sample M-7905/190.6 contains clay mineral of kaolinite group, most likely kaolinite or dickite (Fig. 12c), which associates with calcite, native gold, and chalcopyrite (Fig. 8k).

5.2 Chlorite chemistry and geothermometry

Chlorite is present in most samples with Au-Ag mineralization and shows extremely wide chemical variations (Table 5, Fig. 13), sometimes even within one grain. For example, in the sample M-52/67.1 (see Fig. 3i), early chlorite (Chl-1), which is related to propylitic alteration, is owergrown by chlorite-2 (Chl-2). The latter associates with gold-telluride mineralization (native gold, melonite, and altaite which overgrow cobaltite and chalcopyrite). Chlorite-1 belongs to the clinochlore-daphnite series; it is featured by wide X(Mg) variations (from 0.4 to 0.7) and relatively narrow Si/Al range (1.0–1.1). Chlorite-2 differs from chlorite-1 in higher Si/Al ratio (over 1.2) and narrower X(Mg) range (0.5 to 0.6). Chlorite from other samples with Au-Ag mineralization are also distinguished by highly variable Si/Al ratio (1.1 to 1.8) while X(Mg) and usually remains almost constant for each sample (Fig. 13a), e.g. 0.6 to 0.7 for sample M-50/95.2. In some cases (e.g. in samples M-10405/145 and M-50/95.2), chlorites are featured by a high content of interlayer cations (Ca+Na+K>0.05 apfu) and thus can be referred to as smectite or smectite-illite group. Chlorite from gold-arsenopyrite-base-metal mineralization (sample M-48/138.7) differs from the others in lower X(Mg) (ca. 0.3) but is similar in Si/Al ratio, i.e. 1.3 to 1.5 (Table 5, Fig. 13). Chlorite from argillic alteration (sample Mih-7) has X(Mg) varying from 0.5 to 0.7 and Si/Al 1.1 to 1.3 (Table 5). Temperatures calculated according to Kotelnikov et al. (2012) were within the range 241 to 269^{o}C for chlorite-1 and 177 to 289^{o}C for chlorite-2 and decrease with increase of Si/Al ratio within each sample (Fig. 13b).

6 Fluid inclusion data

Fluid inclusions, appropriate for microthermometric study, were found only in six samples containing precious metal minerals. All observed inclusions were hosted by quartz (in the sample M-5/17 also in calcite) and were considered as primary according to criteria proposed by Roeder

(1984). At room temperature, most fluid inclusions are oval shaped and range from 20 to 30 μm, occasionally up to 40 μm in size.

CL images of vein quartz (Fig. 14) revealed two generations of quartz in most samples: quartz-1 with bright luminescence, sometimes with growth oscillatory zoning (Fig. 14a,b), and quartz-2 with weak luminescence, which overgrows quartz-1 (Fig. 14a) and replaces it via series of cracks (Fig. 14b). Sometimes quartz-2 also shows growth oscillatory zoning, though not so clearly pronounced (Fig. 14f). Quartz-2 coexists with chlorite and most sulfides, i.e. with chalcopyrite and bornite in the sample M1/139 (Fig. 14a,b), and chalcocite in the sample M-5/17 (Fig. 14f).

Samples *M-1/139* and *M-10405/145* contain two types of fluid inclusions of which are confined to quartz-1 (Fig. 14c,d): LV type, and, occasionally of LVS type, both consist of aqueous liquid and vapor bubble (20 vol.%). Inclusions of LVS type contain also the cubic-shaped solid phase up to 5 μm in size. Inclusions of the both types have high salinity (19 to 22 wt.% NaCl-equiv.), an eutectic temperature of –57 to –62^{o}C pointing to the dominance of Ca chlorides and homogenize to liquid phase at 180 to 230^{o}C (Table 5, Fig. 15).

In the *sample M-1-9/15,* three coexisting types of fluid inclusions were identified: (1) VL_1L_2 type fluid inclusions have oval or negative crystal shape and range from 25 to 35 μm in size; they consist of aqueous liquid and vapor bubble (30–40 vol.%) surrounded by a thin rim of carbonic liquid; (2) VLS type fluid inclusions have oval shape and range from 10 to 15 μm in size, consist of aqueous liquid, vapor bubble (30–50 vol.%) and cubic-shaped solid phase up to 5 μm in size; and (3) V type inclusions, 10 to 15 μm in size, consist of vapor. VL_1L_2 and VLS type inclusions show moderate salinity (10 to 11.5 wt.% NaCl-equiv.), an eutectic temperature of –27 to –29^{o}C, pointing to the dominance of Na chlorides with possible admixture of divalent cations (Mg^{2+} or Fe^{2+}), and homogenize to liquid phase at 280 to 320^{o}C (Table 5, Fig. 15).

Samples *M-1/126* and *M-7905/190.6* contain LV-type fluid inclusions 10 to 20 μm in size, consisting of aqueous liquid and vapor bubble (15-20 vol.%), sometimes cubic-shaped solid phase up to 5 μm in size can be observed. Fluid inclusions show low salinity (4 to 8 wt.% NaCl-equiv.) and an eutectic temperature of –28 to –31^{o}C and homogenize to liquid phase at 195 to 220^{o}C.

The sample M-5/17 contains LV-type oval or negative-shaped fluid inclusions 10 to 40 μm in size, hosted by quartz-2 (Fig. 14g,h) and post-ore calcite. Fluid inclusions in quartz homogenize to liquid at 203 to 221^{o}C and establish low- to moderate salinity (6 to 12 wt.% NaCl-equiv.) and an eutectic temperature of –30 to –36^{o}C; fluid inclusions in calcite have low salinity (6 to 9 wt.% NaCl-equiv.) and eutectic temperature of –23 to –22^{o}C and homogenize to liquid at 172 to 183^{o}C (Table 5, Fig. 15).

7 Discussion

7.1 Formation conditions

Fluid inclusion study revealed at least two types of fluids involved in the formation of Au-Ag bearing samples: (1) high saline (19 to 23 wt.% NaCl-equiv.) Ca-Cl rich fluid responsible for formation of the early quartz-1 and (2) low saline (3 to 8 wt.% NaCl-equiv.) NaCl-rich fluid which deposited quartz-2, chlorite, bornite, and chalcopyrite. As no boiling or CO_2 effervescence was observed from all investigated fluid inclusion samples, the obtained homogenization temperature (T_h) may be considered as a minimum entrapment temperature. Although pressure could not be estimated for precious metals bearing samples, we suppose it is similar to that obtained for a propylitic-style host mineralization, i.e. is approx. 110 to 345 Bar (Groznova et al., 2015). Pressure correction for homogenization temperatures (Potter, 1977) will add in this case approx. 30^{o}C. Thus, both fluids were of low-temperature (210 to 260^{o}C). Sample M-9/15 differs from the others in higher temperature (ca. 300^{o}C and higher) and salinity (ca. 11 wt.% NaCl-equiv.), but it is similar in composition to fluid of the second type.

In the sample M-1/126, T_h obtained (195 to 221, mean 211^{o}C, Table 6) is somewhat lower than chlorite geothermometry data (235 to 255, mean 242^{o}C, Table 5) calculated after Kotelnikov et al. (2012). However being corrected for pressure, the entrapment temperature for this sample would make up 225 to 251^{o}C, mean 241^{o}C, which fits well with the chlorite data (table 7). The same is true for samples 7905/190.6 and M-5/17. Thus we can consider the temperature range of ca. 200 to 250^{o}C obtained from both fluid inclusions and chlorite geothermometry as depositional temperature of bornite-chalcopyrite assemblage, hosting gold-silver-telluride mineralization. Chlorite from argillic altered rock (sample Mikh-7) also fits within this interval. The obtained temperatures and the salinity are typical for a dominantly intermediate sulfidation epithermal environment (Sillitoe and Hedenquist, 2003 and refs. therein). Moreover, similar temperature and salinity intervals as well as the evolution from Na-chlorite to Ca-chlorite rich fluids and backward was described for subepithermal veins of the Mt. Milligan porphyry Cu-Au deposit (LeFort et al., 2011).

7.2 Diversity Au and Ag minerals

Native gold is the most common gold mineral in ores of the Mikheevskoe deposit, while Ag tellurides (hessite and, at a lesser degree, stützite) are most typical for silver. Au-Ag tellurides are rare and occur within bornite-chalcopyrite ore and in argillic altered rocks, while Au-Ag selenides were found only in argillic altered rocks. Such a group of minerals is not uncommon for porphyry

copper deposits worldwide. According to the USGS database (Singer et al., 2008), native gold and/or electrum were reported in over 200 out of 678 porphyry copper deposits. However only 17 of those contain Au-Ag tellurides, including 12 findings of hessite (at 7 deposits hessite was the only telluride reported).

Usually the early generation of native gold is confined to bornite and was formed as a result of an exsolution of a high-temperature bornite solid solution (Simon et al., 2000). This gold is normally of high fineness (Sillitoe, 2010). Later generations of gold related to epithermal mineralization may occur within both high- and intermediate sulfidation assemblages and its fineness is more variable, moreover, it often associates with various tellurides. Such mineral sequences were described in the Baimka Cu-porphyry zone, Chukotka (Nikolaev et al., 2016), Bugdaya Mo-porphyry deposit (Kovalenker et al., 2010), Elatsite Cu-porphyry deposit, Bulgaria (Tarkian et al., 2003), Petropavlovskoe Au-porphyry deposit (Vikent'ev at al., 2017) and many others.

In case of the Mikheevskoe deposit, high-fineness gold (ca. 870) in bornite was observed only in the sample M-1/142 (Fig. 3d). All gold grains observed in this sample are oval, supporting the exsolution from bornite. However the elongated shape as well as being confined to bornite margins suggests an overprinting by later processes. In all the other samples native gold and tellurides overgrow earlier sulfides (mainly bornite and chalcopyrite), or are confined to cracks and grain boundaries, and, thus, establish a clearly overlapping relationship with potassic-related bornite-chalcopyrite mineralization (Figs. 3f-k, 4a,e). The observed variety of Te minerals is typical for mineralization of a low to intermediate sulfidation style (Sillitoe and Hedenquist, 2003 and refs. therein). The presence of illitic mica as well as kaolinite is also typical for an epithermal stage of a porphyry system (Arribas et al., 1995; Marushchenko et al., 2015; Parry et al., 2002 and refs. therein) and for shallow (epithermal) levels of porphyry systems (Maydagán et al., 2018), moreover it often contains some paragonitic end-member (Hikov, 2014). However, the absence of base-metal minerals (except of rare galena) suggests that the precious metal minerals represent rather a transitional porphyry to epithermal stage and can be referred to subepithermal mineralization (Sillitoe, 2010; LeFort et al., 2011).

Mineralization of gold-arsenopyrite-base metal type which has a cross-cutting relationship with porphyry-style mineralization (Fig. 8a) and is featured by an abundant sphalerite, galena, tetrahedrite, and arsenopyrite can be ascribed to an intermediate sulfidation style (Sillitoe and Hedenquist, 2003). However, it differs from other Au-Ag mineralization of the Mikheevskoe deposit in white mica chemistry (muscovite-paragonite series with no illite end-member) as well

as in association with dolomite-ankerite series. Chlorite in this mineralization (sample M-48/137.8) also differs from other studied chlorites of in the dominance of the daphnite end-member (X(Mg)=0.3). This, along with higher homogenization temperature obtained for the sample M-9-1/15, might suggest the mineralization of gold-arsenopyrite-base-metal type is linked to another hydrothermal event different from an epithermal stage of a porphyry system evolution.

The set of minerals, comprising argillic alteration (i.e. quartz, illite/hydromica, chlorite, carbonates, kaolinite, roughly corresponds to intermediate argillic alteration typical for porphyry systems (Seedorf et al., 2005 and references therein). It is notable that argillic altered rocks contain almost the same set of Au-Ag minerals and Pb, Bi, Hg tellurides as the bornite-chalcopyrite ore, with the only difference that Se-bearing phases were observed only in argillic altered rocks. Range of gold composition in all types of Au-Ag mineralization is also similar, making two intervals of 0 to 30 and 50 to 80 at.% of Ag (Fig. 11). This indicates that most Au-Ag minerals of the Mikheevskoe deposit, if not all, are related to epithermal overprinting.

It can be assumed that most of precious metals minerals, including native gold and electrum as well as various tellurides deposited at a temperature range from 200 to 300^{o}C. Since all observed telluride-bearing assemblages of the gold-silver-telluride mineralization overlap bornite-chalcopyrite and bornite-chalcocite assemblages they can be supposed to form at the lowest obtained temperature, e.g. ca. 200^{o}C. Thus, most gold and silver bearing assemblages can be discussed in terms of fS_2–fTe_2 at the average temperature of 200^{o}C (Fig. 16a). The main features of Au–Ag mineralization are: (1) they formed within either pyrite-bornite or pyrite–chalcopyrite stability limits; (2) native gold or electrum assemblages formed below the Au/$AuTe_2$ buffer are more widespread than Au-Ag-ditellurides assemblages. Therefore, the observed variability in Au and Ag minerals can be a result of small fluctuations of S_2 and/or Te_2 fugacity. Native gold in tetrahedrite (gold arsenopyrite-base-metal type, sample M-1-9/15) is assumed to precipitate at ca. 300^{o}C (Fig. 16b).

7.3 Significance of PGE minerals

Palladium tellurides (merenskyite and sopcheite), found during this study, were reported in other porphyry copper deposits though they are extremely rare. Merenskyite is the most common PGE mineral in porphyry copper deposits (Tarkian and Stribrny, 1999), e.g. at Elatsite, Bulgaria (Tarkian et al., 2003; Bogdanov et al., 2005), Skouries, Greece (Eliopoulos et al., 2014), Majdanpek, Serbia (Tarkian and Stribrny, 1999), Aksug, Russia (Berzina et al., 2007). In addition, unidentified palladium tellurides were observed at Batu Hijau, Indonesia (Imai and Ohno, 2005) and Bingham, USA (Core et al., 2006). Kovalenker et al. (1996) reported erlichmanite (OsS_2) and moncheite

($Pt(Te,Bi)_2$) in the Ryabinovyi porphyry copper deposit, Central Aldan, Russia, while Sidorov et al. (2017) identified merenskyite, kotulskite ($Pd(Te,Bi)_{2-x}$), keithconnite ($Pd_{20}Te_7$), and temagamite (Pd_3HgTe_3) in the Kirganik porphyry copper deposit, Kamchatka. The highest variety of PGE minerals was described at the Santo Tomas II deposit, Philippines, where Piestrzynski et al. (1994) found merenskyite, vysotskite ((Pd,Ni)S), stibiopalladinite/mertieite (Pd_5Sb_2), kotulskite, and sopcheite. Usually PGE minerals associate with hessite and/or electrum in bornite-chalcopyrite ores. Unfortunately at most of the deposits listed above, PGE minerals were found only in sulfide concentrates and this prevents the estimation of their position in the mineral sequence. Nevertheless, where observed, PGE minerals demonstrate overgrowing textural relationships with earlier bornite-chalcopyrite assemblages (Piestrzynski et al., 1994; Eliopoulos et al., 2014; Sidorov et al., 2017, etc.) and, thus, were formed at the latest stages of the porphyry system. Moreover LeFort et al. (2011) reported a diversity of PGE minerals in association with electrum, tellurides of Ag and Bi and base-metal sulfides in subepithermal veins of the Mount Milligan Cu-Au porphyry deposit.

Economou-Eliopoulos (2005) noted presence of mafic rocks at most porphyry deposits with PGE minerals or elevated PGE content. In case of the Mikheevskoe deposit, hosting basalts intruded by numerous serpentinite bodies could have served as PGE sources. As noted by Economou-Eliopoulos et al. (2017), elevated contents of PGE as well as PGE minerals associate mostly with intrusions with a mantle-derived magma source. High contents of Re in molybdenite of hundreds to thousands ppm (Grabezhev, 2013; Plotinskaya et al., 2015; Tessalina and Plotinskaya, 2017) are in agreement with a noted input of a mafic component. The latter is also confirmed by Nd isotopic data for diorite of the Mikheevsky complex ($\varepsilon Nd = 3.4–4.1$) reported by Grabezhev (2009).

8 Summary

Precious metals (Au, Ag, PGE) in ores of the Mikheevskoe porphyry copper deposit occur in three types of mineralization:

(1) Gold-silver-telluride mineralization confined to porphyry-style bornite-chalcopyrite ores; it includes native gold, electrum, tellurides of Ag, Hg, Bi, Pb, Ni, and Pd and is ascribed to a transitional porphyry-epithermal type.

(2) Gold-arsenopyrite-base-metal mineralization in quartz-tetrahedrite-sphalerite veins cutting porphyry-style mineralization, ascribed to an intermediate-sulfidation type.

(3) Gold-telluride mineralization related to an intermediate argillic alteration is mineralogically similar to that of the type (1) but is distinct in the presence of Au-Ag, Ag, Pb selenides.

Fluid inclusions data and chlorite geothermometry yield a formation temperature of 350 to 170^{o}C, which gives evidence that precious metal minerals at the deposit are linked to epithermal overprinting of the porphyry mineralization.

The observed variability in Au and Ag minerals results from small fluctuations of S_2 and/or Te_2 fugacity.

Acknowledgements

The authors would like to thank the staff of the Russian Copper Company and personally G.K. Yamshchikov for guidance at the deposit as well as A.I. Grabezhev and B.M. Shargorodsky for providing gold-bearing samples. D.B. Bondar (IGEM RAS) is acknowledged for assistance during fieldwork and for critical comments. I.G. Griboedova (IGEM RAS, Moscow), A.N. Nekrasov (IEM RAS, Chernogolovka), I.A. Blinov (IMin UB RAS, Miass), S.P. Glavatskikh (IGG UB RAS, Yekaterinburg), A. Kearsly and T. Salge (NHM, London) are warmly thanked for their assistance with SEM and microprobe analysis. N.G. Petrishcheva and T.Ya. Gulyaeva (IGG Ub RAS, Yekaterinburg) are acknowledged for X-ray and TG/DTA analysis.

Constructive reviews of two anonymous reviewers are greatly appreciated. A. Yakubchuk is warmly thanked for the editorial handling.

This study was supported by NHM (via the CERCAMS Fellowship Program), by the Presidium of the Russian Academy of Sciences, Program No. 48 and, partly, by the Russian Foundation for Basic Research, Project No. 16-05-00622. RS acknowledges funding under NERC Grant NE/P017452/1 “From arc magmas to ores (FAMOS): A mineral systems approach”.

References

Afifi, A.M., Kelly, W.C., Essene, J., 1988. Phase relations among tellurides, sulfides, and oxides: I. Thermochemical data and calculated equilibria. Econ. Geol. 83, 377–394.

Arribas Jr., A., Hedenquist, J.W., Itaya, T., Okada, T., Concepción, R.A., Garciam Jr., J.S., 1995. Contemporaneous formation of adjacent porphyry and epithermal Cu-Au deposits over 300 ka in northern Luzon, Philippines. Geology. 23, 337–340.

Azovskova, O.B., Rovnushkin, M.Y., Glavatskikh, S.P., 2015. Mineralogy of argillic altered rocks from the Mikheevskoe porphyry copper deposit, South Urals. Metallogeny of ancient and modern oceans−2015. 21, 116−120. (in Russian).

Barton Jr., P.B., Skinner, B.J., 1979. Sulfide mineral stabilities. In: Barnes, H.L. (Ed.), Geochemistry of Hydrothermal Ore Deposits. Wiley Interscience, New York, pp. 278–403.

Belgorodskii, E.A., Cherkashev, S.A., Grabezhev, A.I., Shargorodskii, B.M., 1991. The Novonikolaevsk ore cluster. UrB AS USSR, Sverdlovsk (in Russian).

Berzina, A.N., Korobeinikov, A.F., 2007. Rhenium and precious metal (Pt, Pd, and Au) abundances in porphyry Cu-Mo deposits of Central-Asian Mobile Belt. Acta Petrol. Sin. 23(8), 1957−1972.

Berzina, A.N., Sotnikov, V.I., Economou-Eliopoulos, M., Eliopoulos, D.G., 2007. First finding of merenskyite (Pd,Pt)Te_2 in porphyry Cu-Mo ores in Russia. Russ. Geol. Geoph. 48, 656–658.

Bodnar, R.J., Vityk, M.O., 1994. Interpretation of microthermometric data for H_2O–NaCl fluid inclusions. In: De Vivo, B., Frezzotti, M.L. (Eds), Fluid Inclusions in minerals, methods and Applications. Virginia Tech, Blacksburg, VA, pp. 117–130.

Bogdanov, K., Filipov, A., Kehayov, R. 2005. Au-Ag-Te-Se minerals in the Elatsite porphyry-copper deposit, Bulgaria.Proc. Au-Ag-Te-Se deposits, IGCP Project 486, 2005 Field Workshop, Kiten, Bulgaria Geochem. Miner. and Petrol. 42. 13–19.

Cathelineau, M., 1988. Cation Site Occupancy in Chlorite and Illites as a Function of Temperature. Clay Minerals. 23, 471–485.

Core, D.P., Kesler, S.E., Essene, E.J., 2006. Unusually Cu-rich magmas associated with giant porphyry copper deposits: Evidence from Bingham, Utah. Geology, 34(1), 41–44.

Crawford, M.L., 1981. Phase equilibria in aqueous fluid inclusions. In: Hollister, L.S., Crawford, M.L. (Eds), Fluid Inclusions: Applications to Petrology, vol. 6. Mineralogical Association of Canada Short Course Handbook, pp. 75–100.

Economou-Eliopoulos, M., 2005. PGE potential of porphyry deposits. In: Mungall, J.E. (Ed), Exploration for deposits of platinum group elements, short course series. Mineralogical Association of Canada, 25, 203–246

Eliopoulos, D.G., Economou-Eliopoulos, M., Zelyaskova-Panayiotova, M., 2014. Critical factors controlling Pd and Pt potential in porphyry Cu-Au deposits: Evidence from the Balkan Peninsula. Geosciences. 4(1), 31–49.

Economou-Eliopoulos, M., Eliopoulos, D.G., Tsoupas, G., 2017. On the diversity of the PGE content in chromitites hosted in ophiolites and in porphyry-Cu systems: Controlling factors. Ore Geol. Rev. 88, 156–173.

512 Imai, A., Ohno, S., 2005. Primary ore mineral assemblage and fluid inclusion study of the Batu
513 Hijau porphyry Cu-Au deposit, Sumbawa, Indonesia. Resour. Geol. 55, 239–248.
514 Grabezhev, A.I., 2009. Sr–Nd–C–O–H–S isotope-geochemical description of South Urals porphyry-
515 copper fluid-magmatic systems: probable sources of matter. Lithosphere (Russia). 9 (6), 66–
516 89 (in Russian with English abstract).
517 Grabezhev, A.I., 2013. Rhenium in Porphyry Copper Deposits of the Urals. Geol. Ore Deposit. 55,
518 13−26.
519 Grabezhev, A.I., 2014. Novonikolaevsk (Mo,Au)-Cu-porphyry ore area (Southern Ural, Russia):
520 pertochemistry of ore-bearing granitoids and metasomatites. Lithosphere (Russia). 14 (2),
521 60–76 (in Russian with English abstract).
522 Grabezhev A.I., Bakhtina A.P., 1991. Paragonite-bearing metasomatites of the porphyry copper
523 deposits (Novonickolaevsky ore-field, the South Urals). Zap. Vses. Mineral. Ob. 120, 51–58
524 (in Russian with English abstract).
525 Grabezhev, A.I., Belgorodskii, E.A., 1992. Ore-bearing granitoids and metasomatites of copper
526 porphyry deposits. Nauka, Yekaterinburg (in Russian).
527 Grabezhev, A.I., Ronkin, Y.L., 2011. U-Pb age of zircons from ore-bearing granitoids of the South
528 Urals porphyry-copper deposits. Lithosphere (Russia). 11(3), 104–116 (in Russian with
529 English abstract).
530 Grabezhev, A.I., Korobeinikov, A.F., Pshenichkin, F.Y., 2013. Precious metals and rhenium in
531 sulfides from copper-porphyry deposits of the Urals. Yearbook-2012, proc. of the Zavaritsky
532 Institute of Geology and Geochemistry UB RAS. 160, 246–248 (in Russian).
533 Groznova, E.O., Plotinskaya, O.Y., Abramov, S.S., Borovikov, A.A., Milovska, S., Luptakova, J.,
534 Seltmann, R., 2015. Porphyry and Epithermal Deposits of the Urals: PTx-parameters, in:
535 European Current Research on Fluid Inclusions (ECROFI-XXIII). School of Earth and
536 Environment, University of Leeds, pp. 70–71.
537 Hammarstrom, J.M., Mihalasky, M.J., Ludington, S., Phillips, J.D., Berger, B.R., Denning, P.D.,
538 Dicken, C.L., Mars, J.C., Zientek, M.L., Herrington, R.J., Seltmann, R., 2017. Undiscovered
539 porphyry copper resources in the Urals—A probabilistic mineral resource assessment. Ore
540 Geol. Rev. 85, 181–203.
541 Hikov, A., 2014. Paragonite and paragonitic altered rocks from the Asarel porphyry copper deposit,
542 Central Srednogorie. Cr. Acad. Bulg. Sci. 67(8), 1119–1128.
543 Kesler, S.E., Chryssoulis, S.L., Simon, G., 2002. Gold in porphyry copper deposits: Its distribution
544 and fate. Ore Geol. Rev. 21, 103−124.

Kotelnikov, A.R., Suk, N.I., Kotelnikova, Z.A., Tschekina, T.I., Kalinin, G.M., 2012. Mineral geothermometers for low temperature paragenesis. Vestn. Otdelenia nauk Zemle RAN. 4, NZ9001, doi:10.2205/2012NZ_ASEMPG.

Kovalenker, V.A., Myznikov, I.K., Kochetkov, A.Y., Naumov, V.B., 1996. PGE-bearing gold-sulfide mineralization in the Ryabinovyi alkaline massif, Central Aldan, Russia. Geol. Ore Dep. 38, 307–317.

Kovalenker V.A., Kiseleva G.D., Krylova T.L., Andreeva O.V., 2011. Mineralogy and ore formation conditions of the Bugdaya Au-bearing W–Mo porphyry deposit, Eastern Transbaikal Region, Russia. Geol. Ore Deposit. 53, 93–125.

Kranidiotis, P., MacLean, W.H., 1987. Systematics of chlorite alteration at the Phelps Dodge massive sulfide deposit, Matagami, Quebec. Econ. Geol. 82, 1898–1911.

LeFort, D., Hanley, J., Guillong, M., 2011. Subepithermal Au-Pd mineralization associated with an alkalic porphyry Cu-Au deposit, Mount Milligan, Quesnel Terrane, British Columbia, Canada. Econ. Geol. 106, 781–808.

Marushchenko, L.I., Baksheev, I.A., Nagornaya, E.V., Chitalin, A.F., Nikolaev, Y.N., Kalko, I.A., Prokofiev, V.Y., 2015. Quartz–Sericite and Argillic Alterations at the Peschanka Cu–Mo–Au Deposit, Chukchi Peninsula, Russia. Geol. Ore Dep. 57, 213–225.

Maydagán, L., Franchini, M., Impiccini, A., Lentz, D., Patrier, P., Beaufort, D., 2018. Chlorite, white mica and clay minerals as proximity indicators to ore in the shallow porphyry environment of Quebrada de la Mina deposit, Argentina. Ore Geol. Rev. 92, 297–317.

Meunier, A., 2005. Clays. Springer, Berlin.

Nikolaev, Y.N., Baksheev, I.A., Prokofiev, V.Y., Nagornaya, E.V., Marushchenko, L.I., Sidorina, Y.N., Chitalin, A.F., Kalko, I.A., 2016. Gold–Silver Mineralization in Porphyry–Epithermal Systems of the Baimka Trend, Western Chukchi Peninsula, Russia. Geol. Ore Dep. 58, 284–307.

Parry, W.T., Jasumback, M., Wilson, P.N., 2002. Clay mineralogy of phyllic and intermediate argillic alteration at Bingham, Utah. Econ. Geol. 97, 221–239.

Pašava, J., Vymazalová, A., Košler, J., Koneev, R.I., Jukov, A.V., Khalmatov, R.A., 2010. Platinum-group elements in ores from the Kalmakyr porphyry Cu–Au–Mo deposit, Uzbekistan: bulk geochemical and laser ablation ICP-MS data. Miner, Deposita. 45, 411–418.

Piestrzynski, A., Schmidt, S., Franco, H., 1994. Pd-minerals in the Sto. Tomas II, porphyry copper deposit, Tuba Benguet, Philippines. Mineral. Polonica. 25(2), 21–31.

Plotinskaya, O.Y., Grabezhev, A.I., Seltmann, R., 2015. Rhenium in ores of the Mikheevskoe Mo-Cu porphyry deposit, South Urals. Geol. Ore. Deposit. 57, 118−132.

578 Plotinskaya, O.Y., Grabezhev, A.I., Tessalina, S., Seltmann, R., Groznova, E.O., Abramov, S.S., 2017.
579 Porphyry deposits of the Urals: geological framework and metallogeny. Ore Geol. Rev. 85,
580 153–173.
581 Potter II, R.W., 1977. Pressure correction for fluid-inclusion homogenization temperatures based
582 on the volumetric properties of the system NaCl–H_2O. Jour. Research U.S. Geol. Survey. 5(5),
583 603–607.
584 Puchkov, V.N., 2017. General features relating to the occurrence of mineral deposits in the Urals:
585 What, where, when and why. Ore Geol. Rev. 85, 4–29.
586 Roeder, E., 1984. Fluid inclusions. Rev. Mineral. 12.
587 Russian Copper Company. http://rmk-group.ru/en/activities/enterprises/mikheevsky/ (accessed
588 04/01/2018).
589 Samygin, S.G., Burtman, V.S., 2009. Tectonics of the Ural Paleozoides in comparison with the Tien
590 Shan. Geotectonics. 43, 133−151.
591 Seedorff, E., Dilles, J.H., Proffett, J.M., Jr., Einaudi, M.T., Zurcher, L., Stavast, W.J.A., Johnson, D.A.,
592 Barton, M.D., 2005. Porphyry deposits: Characteristics and origin of hypogene features.
593 Econ. Geol. 100, 251−298.
594 Seltmann, R., Porter, T.M., Pirajno, F., 2014. Geodynamics and metallogeny of the Central Eurasian
595 porphyry and related epithermal mineral systems: a review. J. Asian Earth Sci. 79, 810–841.
596 Shargorodskii, B.M., Novikov, I.M., Aksenov, S.A., 2005. The Mikheevskoe copper porphyry deposit
597 in the South Urals. Otechestvennaya Geologia (2), 57–61 (in Russian).
598 Sillitoe, R.H., 2010. Porphyry copper systems. Econ. Geol. 105, 3−41.
599 Sillitoe, R.H., Hedenquist, J.W., 2003. Linkages between volcanotectonic settings, ore fluid
600 compositions, and epithermal precious metal deposits. Soc. Econ. Geol. Spec. Publ. 10, 315–
601 343.
602 Sidorov, E.G., Ignatyev, E.K., Chubarov, V.M., 2017. First Find of Platinum Group Metals in the Ore
603 of Kirganik Copper–Porphyry Deposit (Kamchatka). Dokl. Earth Sci. 475(2), 883–886.
604 Singer, D.A., Berger, V.I., Moring, B.C., 2008. Porphyry Copper Deposits of the World: Database
605 and Grade and Tonnage Models. U.S. Department of the Interior, U.S. Geological Survey,
606 Open-File, Report, pp. 2008–1155.
607 Simon, G., Kesler, S.E., Essene, E.J., Chryssoulis S.L., 2000. Gold in porphyry copper deposits:
608 Experimental determination of the distribution of gold in the Cu-Fe-S system at 400° to
609 700°C. Econ. Geol. 95, 259−270.

610 Sotnikov, V.I., Berzina, A.N., Economou-Eliopoulos, M., Eliopoulos, D.G., 2001. Palladium, platinum
611 and gold distribution in porphyry Cu ± Mo deposits of Russia and Mongolia. Ore Geol. Rev.
612 18, 95–111.
613 Tarkian, M., Stribrny, B., 1999. Platinum-group elements in porphyry copper deposits: a
614 reconnaissance study. Mineral. Petrol. 65, 161–183.
615 Tarkian, M., Hünken, U., Tokmakchieva, M., Bogdanov, K., 2003. Precious-metal distribution and
616 fluid-inclusion petrography of the Elatsite porphyry copper deposit, Bulgaria. Miner.
617 Deposita. 38, 261–281.
618 Tessalina, S.G., Plotinskaya, O.Y., 2017. Silurian to Carboniferous Re-Os molybdenite ages of the
619 Kalinovskoe, Mikheevskoe and Talitsa Cu-Mo porphyry deposits in the Urals: implications for
620 geodynamic setting. Ore Geol. Rev. 85, 174–180.
621 Vestnik Zolotopromyshlennika, 2017. https://gold.1prime.ru/news/20170920/226023.html
622 (accessed 01/12/2017) (in Russian).
623 Vikent'ev, I.V., Mansurov, R.Kh., Ivanova, Yu.N., Tyukova, E.E., Sobolev, I.D., Abramova, V.D.,
624 Vykhristenko, R.I., Trofimov, A.P., Khubanov, V.B., Groznova, E.O., Dvurechenskaya, S.S.,
625 Kryazhev, S.G., 2017. Porphyry-Style Petropavlovskoe Gold Deposit, the Polar Urals:
626 Geological Position, Mineralogy, and Formation Conditions. Geol. Ore Deposit. 59, 482–520.
627 Volchkov, A.G., Kuznetsov, V.V., Nikeshin, Y.V., 2015. Tasks and targets of the national budget
628 funded geological exploration for base metals (Cu, Pb, Zn). Rudy i Metally (1), 30–35 (in
629 Russian with English abstract).
630

Figures

Fig. 1. Geological map of the Mikheevskoe deposit (after Shargorodskii et al., 2005).

Fig. 2. Cross-section along the A-A' line (a) and Cu content map (b), simplified after Shargorodskii et al. (2005); see Fig. 1 for legend.

Fig. 3. Native gold in bornite; SEI – secondary electron images, others – reflected light.
a to c – hand specimens: a – 46/245, b –1/139, c –10405/154; d – native gold (Au) and galena (Gn) in bornite (Bn) surrounded by quartz (Qtz), sample M-1/142; e and f – native gold with petzite (Ptz) in bornite overgrown with epidote (Ep), sample M-46/245, g and h – native gold with krennerite (?) (Kr) and Bi sulfide (Bis) surrounded by chlorite (Chl), titanite (Tit) and epidote, sample M-10405/145; i to k – native gold, melonite and altaite with cobaltite-gersdorffite (Co) and chalcopyrite (Ccp), sample M-52/67.1.

Fig. 4. Tellurides of Ag, Bi, and Hg in bornite and chalcopyrite; e– reflected light, others– secondary electron images.
a – Bi telluride or sulfotelluride (Bi-Te) and native tellurium (Te) on the boundary of chalcopyrite and bornite, sample M-10405/145; b – stützite in bornite, sample M-46/245a; c – stutzite (St) and native tellurium in bornite, sample M-1/126; d – altaite, stützite, and coloradoite (Col) in bornite, sample M-1/126; e and f – hessite (Hs), coloradoite, kawazulite (Kaw), and tetradymite on the quartz-chalcopyrite boundary, sample M-50/95.2; g – coloradoite in bornite, sample M-1/126.

Fig. 5. Silver telluride in molybdenite (Mo), sample M-46/245.
a – reflected light, others – secondary electron images.

Fig. 6. Hessite with palladium tellurides, sample M-1/139. a and c – reflected light, others-secondary electron images.
Mer– merenskyite, Sop– sopcheite, Ptz– petzite, sample M-1/139.

Fig. 7. Gold-silver-telluride mineralization in bornite-chalcocite assemblage (sample M5/17). b–reflected light, c-f – secondary electron images.

a– quartz (Qtz) vein with large nest of bornite (Bn), hand specimen; b– chalcocite and calcite (Cal) overgrow bornite; c– enlarged fragment of (b), chalcocite (Cct) overgrows bornite and forms myrmekitic inclusions in it; hessite (Hs) forms a chain of inclusions in bornite, tetrahedrite (Td) owergrows both chalcocite and bornite; d– galena (Gn) forms "chains" of micron-scale inclusions tracing fractures in bornite; e– hessite and galena are confined to the border of a chalcocite droplet in bornite; f– inclusions of hessite and low-fineness electrum (Au600) in bornite.

Fig. 8. Gold-arsenopyrite-base metal mineralization.

a - quartz-base-metal veins in the open pit; b-d – sample M3-1/16, b – electrum with arsenopyrite and sphalerite; argentoan tetrahedrite and polybasite overgrowing chalcopyrite; e-I − gold in tetrahedrite (Td) and arsenopyrite (Asp), sample M1-9/15; j-l − gold with pyrite and chalcopyrite in calcite (Cal), sample M-7905/190.6.

Fig. 9. Telluride and selenide mineralization overgrowing sulfides from zones of intense argillic alteration (back-scattered electron images).

a – argillic alteration in the open pit; b-(a) − Au-Ag-selenides ((Au-Ag)-Sel) with inclusions of electrum (Elc, bright spots) on chalcopyrite (Ccp), sample Mikh-14-1, zone Arg-1; c − naumannite (Nm) and Cu-Ag-selenide ((Cu-Ag)-Sel) on pyrite (Py) surface, sample Mikh-16, weathering crust; d − mixture of Bi-Ag-Te-Se-phases intergrown with hessite (Hs), chalcopyrite (Ccp) and Ni-alloclasite (Co) on pyrite surface, sample Mikh-7, zone Arg-1; e,f − hessite and «sponge-like» mixture of Ag and Cu tellurides, selenides and, presumably, sulfoselenides (Sel-Tel-(Ag,Bi)), confined to chalcopyrite inclusions in pyrite, sample Mikh-T-1, zone Arg-1; g − Se- and Cu-bearing galena (Gn(Se,Cu)) on pyrite, sample Mikh-T-3, zone Arg-2; h − mixture of Pb, Bi, and Hg tellurides, sample Mikh-7, zone Arg-1; i– hessite (Hs) on pyrite surface, sample Mikh-T-2, zone Arg-2.

Fig. 10. Native gold from loose argillic altered rock (back-scattered electron images).

a, b – Hg-bearing electrum (Elc(*Hg*)) on pyrite grain of complicated morphology, sample Mikh-7, zone Arg-1; c − native gold of high fineness with low-temperature bitumen (Bit), sample Mikh -T-3, zone Arg-2; d − native gold on pyrite, sample Mikh-7, zone Arg-1; e − pyrite with inclusions of cobaltite (Co) and native gold, sample Mikh-7, zone Arg-1. Telluride and selenide mineralization in aureoles of argillic alteration (polished sections, back-scattered electron images). f − hessite (Hs) and coloradoite (Col) in chalcopyrite (Ccp) veinlet cutting pyrite, sample Mikh-9.

Fig. 11. Histograms of Ag contents (at.%) in native gold from different types of mineralization.

Fig. 12. Diagrams $Mg+Fe^{2+}$ versus Si (a), X(Na) versus Si, (b), and 2R3–MR3–3R2 (c) for micas associated with precious metals mineralization. MR3 = (K+Na+2Ca), R3 = ($Al + Fe^{3+}$), R2 = ($Mg+Fe^{2+}$+Mn) (Meunier, 2005)

Fig. 13. Diagrams X(Mg) versus Si/Al and Si/Al versus Temperature calculated after Kotelnikov et al. (2012) for chlorites associated with precious metals mineralization.

Fig. 14. Fluid inclusions from quartz with precious metals mineralization. a and b – BSE and CL images of quartz hosting bornite, chalcopyrite, and chlorite, sample M-1/139. Note that sulfides and chlorite are confined to later (dark) quartz 2. c-e– LV-type fluid inclusions: c–sample M-1/139, d – sample M-10405/154, e – sample M-1-9/15.

Fig. 15. Homogenization temperature vs salinity (a) and vs eutectic temperature (b) diagrams for quartz from gold-telluride-bearing assemblages of the Mikheevskoe deposit

Fig. 16. LogfS_2 vs. logfTe_2 diagram of the major gold and silver bearing assemblages of the Mikheevskoe deposit for a temperature of 200°C (a) and 300°C (b). Thermodynamic data from (Barton and Skinner, 1979; Afifi et al., 1988).
Assemblages: (1) Native gold+galena in bornite (sample M-1/142) and electrum+hessite+ galena in bornite, sample M-5/17; (2) Au-Ag-telluride+Bi sulfide in bornite (sample M-10405/145), (3) coloradoite, altaite, stützite, native Te, Bi telluride in bornite, samples M-1/126 and M-46/245, (4) krennerite stützite, native Te, galena, hessite, tellurobismuthite, coloradoite in chalcopyrite, sample M-1/139; (5) electrum, melonite, altaite in chalcopyrite, sample M-52/67.1; (6) native gold in tetrahedrite, sample M9-1/15.

Tables

Table 1. Representative microprobe analysis of native gold from the Mikheevskoe deposit

Table 2. Representative EDX analysis of Te and Se minerals from the Mikheevskoe deposit

729 **Table. 3.** Representative EDX analyses of tetrahedrite (Nos 1 to 4), argentoan tetrahedrite (Nos 5
730 to 9), freibergite (Nos 10 and 11), and polybasite (Nos 12 and 13) from gold-arsenopyrite-base-
731 metal mineralization
732
733 **Table 4.** Chemical composition of mica and clay (wt.%) associating with precious metal
734 mineralization
735
736 **Table 5.** Chemical composition of chlorite (wt.%) associating with precious metal mineralization,
737 and calculated temperature (^{o}C)
738
739 **Table 6.** Microthermometric data of fluid inclusions in quartz and calcite from gold-telluride-
740 bearing assemblages of the Mikheevskoe deposit
741
742 **Table 7.** Comparison of depositional temperatures obtained via chlorite geothermometry and fluid
743 inclusions data
744
745 ## Supplementary data
746 **Appendix A.** Chemical composition of mica and clay mineral (wt.%) associating with precious
747 metal mineralization
748
749 **Appendix B.** Chemical composition of chlorite (wt.%) associating with precious metal
750 mineralization, and calculated temperature (^{o}C)
751

752 **Table 1.** Representative microprobe analysis of native gold from the Mikheevskoe deposit
753

	Sample	Comment	Au	Ag	Hg	Cu	Total	Fine-ness	Formula
1	M-1/142*	in bornite with c galena	85.20	13.48	<d.l.	1.48	100.16	863	$Au_{78}Ag_{22}$
2			85.21	12.44	<d.l.	1.84	99.49	873	$Au_{79}Ag_{21}$
3	M-46/245a*	in bornite with petzite	57.51	37.38	<d.l.	<d.l.	94.89	606	$Au_{46}Ag_{54}$
4	M-46/245a*	in bornite with petzite	59.20	40.58	<d.l.	<d.l.	99.78	593	$Au_{44}Ag_{56}$
5	M-10405/145*	in bornite with krennerite(?)	67.50	32.90	<d.l.	<d.l.	100.40	672	$Au_{53}Ag_{47}$
6	M-52/67.1*	in cobaltite	52.60	14.09	<d.l.	<d.l.	66.68	789	$Au_{67}Ag_{33}$
7	M-5/17*	in bornite + chalcosite with hessite and galena	47.75	40.61	1.48	<d.l.	97.65	535	$Au_{39}Ag_{60}Hg_{1}$
8			62.26	35.10	1.17	<d.l.	98.53	632	$Au_{49}Ag_{50}Hg_{1}$
9			64.56	33.42	0.89	<d.l.	98.86	653	$Au_{51}Ag_{48}Hg_{1}$
1	M-1-9/15	tetrahedrite	75.58	20.65	<d.l.	1.42	97.65	767	$Au_{67}Ag_{33}$
1			78.33	18.82	2.22	0.25	99.61	774	$Au_{68}Ag_{30}Hg_{2}$
1			78.68	17.89	1.09	1.78	99.44	784	$Au_{70}Ag_{29}Hg_{1}$
1	M-6-1/16	tetrahedrite	92.15	5.69	<d.l.	2.58	100.41	916	$Au_{90}Ag_{10}$
1	M-3-1C/16*	galena, sphalerite, arsenopyrite	44.46	52.82	2.33	<d.l.	99.61	446	$Au_{31}Ag_{67}Hg_{2}$
1			51.52	43.15	4.93	<d.l.	99.61	517	$Au_{38}Ag_{58}Hg_{4}$
1			52.66	44.02	4.12	<d.l.	100.80	522	$Au_{38}Ag_{59}Hg_{3}$
1	M-7905/190	in calcite, 100µm x 2 mm	87.35	11.89	<d.l.	<d.l.	99.27	880	$Au_{80}Ag_{20}$
1			86.49	12.13	0.09	<d.l.	98.76	876	$Au_{79}Ag_{19}$
1		in calcite, 100x500 µm	88.66	12.20	<d.l.	<d.l.	100.86	879	$Au_{80}Ag_{20}$
2			86.17	12.24	0.21	<d.l.	98.67	873	$Au_{79}Ag_{21}$
2			86.87	12.24	<d.l.	<d.l.	99.19	876	$Au_{80}Ag_{20}$
2		in calcite, 200 µm	87.57	12.96	0.35	<d.l.	100.92	868	$Au_{78}Ag_{22}$
2			85.55	12.74	0.26	<d.l.	98.58	868	$Au_{78}Ag_{22}$
2		in calcite, intergrown with chalcopyrite, 30 x 100 µm	86.23	12.27	<d.l.	<d.l.	98.55	875	$Au_{79}Ag_{21}$
2			87.20	11.54	0.06	<d.l.	98.88	882	$Au_{80}Ag_{20}$
2		in calcite, 10 µm	89.96	9.03	<d.l.	<d.l.	99.02	909	$Au_{84}Ag_{16}$
2			90.81	8.41	<d.l.	<d.l.	99.35	914	$Au_{85}Ag_{15}$
2	Mikh-7*	on pyrite surface, 2-3 µm	85.39	11.06	<d.l.	<d.l.	96.45	885	$Au_{81}Ag_{19}$
2			23.74	45.64	7.80	<d.l.	77.18	308	$Au_{21}Ag_{73}Hg_{6}$
3	Mikh-14*	on pyrite with chalcopyrite, 5-7 µm	49.96	35.09	<d.l.	<d.l.	85.05	587	$Au_{44}Ag_{56}$
3	Mikh-T-3*	on pyrite with bitumen , 5x15 µm	60.91	<d.l.	<d.l.	<d.l.	60.91	1000	Au_{100}

754 *– EDX analysis; <d.l. – below detection limit (ca. 0.04 wt.% for WDX analyses and ca. 0.5 wt.% for
755 EDX analyses); formulae calculated for 100 atoms
756

757 **Table 2.** Representative EDX analysis of Te and Se minerals from the Mikheevskoe deposit
758
759

Sample	Comment	Au	Ag	Hg	Bi	Pb	Ni	Pd	Fe	Te	Se	S	Total	Formula
M-46/245a	Petzite	20.59	32.52	–	–	–	–	–	–	29.16	–	–	82.27	$Au_{1.0}Ag_{2.9}Te_{2.2}$
M-46/245a	Stützite	–	58.27	–	–	–	–	–	–	40.67	–	–	98.94	$Ag_{5.0}Te_{3.0}$
M-10405/145	Krennerite?	18.44	3.44	–	–	–	–	–	–	27.56	–	–	49.44	$Au_{1.6}Ag_{0.6}Te_{3.8}$
M-52/67.1	Melonite	–	18.13	–	–	–	83.56	–	–	–	–	–	101.69	$Ni_{1.0}Te_{2.0}$
		–	17.71	–	–	–	83.44	–	–	–	–	–	101.15	$Ni_{0.9}Te_{2.1}$
		–	17.66	–	–	–	83.67	–	–	–	–	–	101.33	$Ni_{0.9}Te_{2.1}$
M-1/139	Stützite	–	56.48	–	–	–	–	–	–	43.56	–	–	100.04	$Ag_{4.6}Te_{3.0}$
		–	58.44	–	–	–	–	–	–	43.02	–	–	101.45	$Ag_{4.8}Te_{3.0}$
		–	58.26	–	–	–	–	–	–	43.14	–	–	101.40	$Ag_{4.8}Te_{3.0}$
	Hessite	–	62.57	–	–	–	–	–	–	37.16	–	–	99.74	$Ag_{2.0}Te_{1.0}$
		–	61.47	–	–	–	–	–	–	38.46	–	–	99.93	$Ag_{2.0}Te_{1.0}$
		–	61.65	–	–	–	–	–	–	36.96	–	–	98.61	$Ag_{2.0}Te_{1.0}$
	Merenskiite	–	–	–	–	–	0.93	26.38	–	70.72	–	–	98.03	$(Pd_{0.9}Ni_{0.1})_{\Sigma 1.0}Te_{2.0}$
	Sopcheite	–	33.52	–	–	–	–	20.64	1.70	41.49	–	–	97.35	$Ag_{4.0}(Pd_{2.5}Fe_{0.4})_{\Sigma 2.9}Te_{4.2}$
M-1/126	Coloradoite	–	–	60.65	–	–	–	–	–	38.07	–	–	98.72	$Hg_{1.0}Te_{1.0}$
	Native Te	–	–	–	–	–	–	–	–	97.84	–	–	97.84	
	Empressite	–	46.92	–	–	–	–	–	–	54.26	–	–	101.18	$Ag_{1.0}Te_{1.0}$
	Stützite	–	57.63	–	–	–	–	–	–	44.02	–	–	101.65	$Ag_{4.9}Te_{3.1}$
	Altaite	–	–	–	–	59.5	–	–	–	40.03	–	–	99.50	$Pb_{1.0}Te_{1.0}$
	Coloradoite	–	–	60.51	–	–	–	–	–	36.99	–	–	97.50	$Hg_{1.0}Te_{1.0}$
M-50/95.2	Kawazulite	–	–	–	55.53	–	–	–	–	35.71	6.85	1.26	99.35	$Bi_{2.0}Te_{2.1}(Se_{0.7}, S_{0.3})_{\Sigma 1.0}$

	Tetradymite	–	–	–	58.75	–	–	–	–	35.70	0.69	3.46	98.60	$Bi_{2.1}Te_{2.1}(Se_{0.1}, S_{0.8})_{\Sigma 0.9}$
		–	–	–	60.21	–	–	–	–	34.86	3.89	2.75	101.72	$Bi_{2.1}Te_{2.0}(Se_{0.4}, S_{0.6})_{\Sigma 1.0}$
	Coloradoite	–	–	61.61	–	–	–	–	–	36.70	–	–	98.31	$Hg_{1.0}Te_{1.0}$
M-1/17	Galena	–	–	–	–	87.17	–	–	–	–	0.60	11.78	99.55	$Pb_{1.06}(S_{0.92}Se_{0.02})_{\Sigma 0.94}$
		–	–	–	–	87.26	–	–	–	–	0.78	11.85	99.89	$Pb_{1.05}(S_{0.92}Se_{0.03})_{\Sigma 0.95}$
	Hessite	–	62.99	–	–	–	–	–	–	37.06	–	–	100.05	$Ag_{2.0}Te_{1.0}$

760

761 – not found

762

763 **Table. 3**. Representative EDX analyses of tetrahedrite (Nos 1 to 4), argentoan tetrahedrite (Nos 5
764 to 9), freibergite (Nos 10 and 11), and polybasite (Nos 12 and 13) from gold-arsenopyrite-base-
765 metal mineralization

No	Cu	Ag	Fe	Zn	As	Sb	S	Total	Formulae calculated for 29 apfu
M1-9/15									
1.	38.88	0.22	4.62	2.40	4.65	23.10	26.36	100.23	$Cu_{9.9}(Fe_{1.3}Zn_{0.6})_{\Sigma 1.9}(Sb_{3.0}As_{1.0})_{\Sigma 4.0}S_{13.2}$
2.	37.52	0.31	4.18	3.23	0.74	27.52	24.77	97.97	$(Cu_{9.9}Ag_{0.1})_{\Sigma 10.0}(Fe_{1.3}Zn_{0.8})_{\Sigma 2.1}(Sb_{3.8}As_{0.2})_{\Sigma 4.0}S_{13.0}$
3.	37.21	0.70	4.98	2.75	3.73	23.76	25.74	98.87	$(Cu_{9.6}Ag_{0.1})_{\Sigma 9.7}(Fe_{1.4}Zn_{0.7})_{\Sigma 2.1}(Sb_{3.2}As_{0.8})_{\Sigma 4.0}S_{13.1}$
M-3-1C/16									
4.	34.29	3.64	1.15	7.53	–	28.61	24.92	100.14	$(Cu_{9.1}Ag_{0.6})_{\Sigma 9.7}(Fe_{0.3}Zn_{1.9})_{\Sigma 2.2}Sb_{4.0}S_{13.1}$
5.	26.73	14.64	5.30	1.48	–	27.45	23.85	99.46	$(Cu_{7.4}Ag_{2.4})_{\Sigma 9.9}(Fe_{1.6}Zn_{0.4})_{\Sigma 2.0}Sb_{4.0}S_{13.1}$
6.	24.82	17.36	5.61	1.50	–	26.95	23.29	99.52	$(Cu_{7.0}Ag_{2.9})_{\Sigma 9.9}(Fe_{1.8}Zn_{0.4})_{\Sigma 2.2}Sb_{4.0}S_{13.0}$
7.	22.21	21.44	5.50	0.89	–	26.46	22.81	99.32	$(Cu_{6.4}Ag_{3.6})_{\Sigma 10.0}(Fe_{1.8}Zn_{0.2})_{\Sigma 2.0}Sb_{4.0}S_{13.0}$
8.	21.27	23.01	4.64	1.89	–	26.77	23.01	100.59	$(Cu_{6.1}Ag_{3.9})_{\Sigma 10.0}(Fe_{1.5}Zn_{0.5})_{\Sigma 2.0}Sb_{4.0}S_{13.0}$
9.	20.96	23.46	6.09	0.43	–	26.21	23.00	100.16	$(Cu_{6.0}Ag_{4.0})_{\Sigma 10.0}(Fe_{2.0}Zn_{0.1})_{\Sigma 2.1}Sb_{3.9}S_{13.0}$
10.	20.21	24.40	5.51	1.14	–	26.36	22.62	100.24	$(Cu_{5.8}Ag_{4.2})_{\Sigma 10.0}(Fe_{1.8}Zn_{0.3})_{\Sigma 2.1}Sb_{4.0}S_{13.0}$
11.	14.76	33.03	4.54	2.01	–	26.01	20.77	101.12	$(Cu_{4.4}Ag_{5.9})_{\Sigma 10.3}(Fe_{1.5}Zn_{0.6})_{\Sigma 2.1}Sb_{4.1}S_{12.4}$
12.	7.84	69.45	–	–	–	7.91	13.25	98.44	$Cu_{1.0}(Ag_{4.1},Cu_{1.9})_{\Sigma 6}Ag_{10.9}Sb_{1.5}S_{9.6}$
13.	8.95	67.05	–	–	–	9.63	15.83	101.46	$Cu_{1.0}(Ag_{3.9},Cu_{2.1})_{\Sigma 6}Ag_{9.6}Sb_{1.7}S_{10.7}$

766
767

768 Table 4. Chemical composition of mica and clay mineral (wt.%) associating with precious metal
769 mineralization (see Appendix A for the full data)

	M-52/67.1			M-3/16			M-5/17			M-7905/190		
Sample	n = 9			n = 7			n = 9			n = 4		
	Min	Max	Mean	Min	Max	Mean	Min	Max	Mean	Min	Max	Mean
SiO_2	47.57	51.04	49.06	46.52	47.20	46.79	46.45	51.02	49.17	45.30	47.10	46.16
TiO_2	<d.l.	0.49	0.18		<d.l.			<d.l.			<d.l.	
Al_2O_3	27.47	32.20	30.46	35.55	39.67	37.59	31.50	33.82	32.30	35.20	36.75	35.92
FeO	1.36	2.92	2.01	<d.l.	0.47	0.13	0.56	1.07	0.84	0.53	0.83	0.67
MgO	1.58	2.73	2.02	<d.l.	0.54	0.13	<d.l.	0.73	0.36	0.31	0.46	0.39
CaO		<d.l.			<d.l.		<d.l.	0.78	0.16	0.42	0.61	0.48
Na_2O	<d.l.	0.30	0.18	0.87	6.27	3.43	1.07	1.58	1.25		<d.l.	
K_2O	10.78	11.71	11.13	2.84	10.40	6.30	5.50	6.23	5.82	0.09	0.33	0.22
Si	3.19	3.40	3.29	2.99	3.14	3.09	3.43	3.56	3.49	1.96	1.98	1.97
Ti	–	0.02	0.01	–	–	–	–	–	–	–	–	–
Al	2.18	2.53	2.41	2.80	3.00	2.92	2.66	2.75	2.71	1.79	1.83	1.81
Al^{IV}	0.60	0.81	0.71	0.86	1.01	0.91	0.44	0.57	0.51	–	–	–
Al^{VI}	1.56	1.78	1.70	1.92	2.05	2.01	2.12	2.27	2.20	–	–	–
Fe'''		0.07	0.03	–	0.03	0.00	–	–	–	0.01	0.03	0.02
Fe''	0.06	0.13	0.09	–	0.03	0.01	0.03	0.06	0.05	–	–	–
Mg	0.16	0.27	0.20	–	0.05	0.01	–	0.08	0.04	0.02	0.03	0.03
Ca	–	–	–	–	0.00	0.00	–	0.06	0.01	0.02	0.03	0.02
Na	–	0.04	0.02	0.11	0.78	0.44	0.15	0.21	0.17	–	–	–
K	0.93	1.01	0.95	0.23	0.89	0.53	0.49	0.56	0.53	0.00	0.02	0.01
X(Na)	–	0.04	0.02	0.11	0.77	0.45	0.21	0.30	0.24	–	–	–

770
771 Formula units calculated on the basis of 7 cations for mica and 7 oxygens for clay
772 Fe was calculated as FeO for mica and Fe_2O_3 for clay
773

Table 5. Chemical composition of chlorite (wt.%) associating with precious metal mineralization, and calculated temperature (^{o}C) (see Appendix B for the full data)

Sample	M-52/67 Chlorite-1			M-52/67 Chlorite-2			M-50/95.2			M-46/245			M-10405/145			M-1/142			M-1/139			M-1/126			M-5/17			M-48/137.8			M-7905/190			Mih-7		
	n = 12			n = 4			n = 18			n = 7			n = 12			n = 15			n = 34			n = 7			n = 18			n = 9			n = 12			n = 4		
	Min	Max	Mean	Min	Max	Mean	Min	Max	Mean	Min	Max	Mean	Min	Max	Mean	Min	Max	Mean	Min	Max	Mean	Min	Max	Mean	Min	Max	Mean	Min	Max	Mean	Min	Max	Mean	Min	Max	Mean
SiO_2	25.67	27.22	26.51	26.82	28.85	27.71	27.11	31.16	28.91	24.78	28.29	26.79	29.08	33.45	30.69	26.40	29.95	28.44	26.51	28.46	27.48	26.87	28.33	27.70	25.40	28.75	27.14	24.52	26.81	26.06	23.90	29.61	27.44	25.21	28.01	26.20
TiO_2	<d.l.	<d.l.	<d.l.	<d.l.	<d.l.	<d.l.	<d.l.	0.49	0.17	<d.l.	<d.l.	<d.l.	0.80	1.24	1.05	<d.l.	<d.l.	<d.l.	<d.l.	<d.l.	<d.l.	<d.l.	<d.l.	<d.l.	<d.l.	<d.l.	<d.l.	0.00	0.00	0.00	<d.l.	<d.l.	<d.l.	<d.l.	<d.l.	<d.l.
Al_2O_3	20.22	21.98	20.93	18.88	19.67	19.16	14.90	20.24	17.30	16.03	18.47	17.42	15.89	20.61	17.92	17.54	20.01	18.65	18.84	20.92	19.54	18.10	20.46	19.43	17.81	21.64	19.51	15.05	16.61	15.78	18.02	22.44	20.06	17.82	21.15	19.62
Cr_2O_3	<d.l.	<d.l.	<d.l.	<d.l.	<d.l.	<d.l.	<d.l.	0.46	0.08	<d.l.	<d.l.	<d.l.	<d.l.	<d.l.	<d.l.	0.23	0.24	0.24	<d.l.	<d.l.	<d.l.	<d.l.	<d.l.	<d.l.	<d.l.	<d.l.	<d.l.	<d.l.	<d.l.	<d.l.	<d.l.	<d.l.	<d.l.	0.59	0.59	0.59
FeO	16.35	28.11	23.04	21.40	24.76	23.29	15.10	20.11	17.76	17.72	23.92	20.62	14.81	17.73	16.16	20.21	24.65	22.42	17.02	22.35	19.99	16.73	17.33	16.89	20.88	25.84	23.35	33.60	35.19	34.36	21.06	30.05	24.58	16.21	26.52	19.11
MnO	<d.l.	0.24	0.08	<d.l.	0.26	0.06	<d.l.	0.28	0.12	<d.l.	0.31	0.11	<d.l.	<d.l.	<d.l.	<d.l.	<d.l.	<d.l.	<d.l.	<d.l.	<d.l.	0.28	0.28	0.28	<d.l.	<d.l.	<d.l.	0.55	0.79	0.64	0.19	0.40	0.28	0.24	0.24	0.24
MgO	11.08	19.13	15.49	14.69	18.42	16.27	18.52	22.84	20.68	14.68	19.07	16.75	21.71	25.01	23.31	15.58	20.53	18.63	18.42	22.20	20.15	19.74	21.88	21.11	14.51	20.06	17.99	7.87	9.48	8.49	12.43	19.61	16.72	13.38	22.10	18.58
CaO	<d.l.	<d.l.	<d.l.	<d.l.	<d.l.	<d.l.	<d.l.	1.50	0.18	<d.l.	<d.l.	<d.l.	0.30	0.67	0.47	0.15	0.15	0.15	<d.l.	<d.l.	<d.l.	<d.l.	<d.l.	<d.l.	<d.l.	<d.l.	<d.l.	<d.l.	<d.l.	<d.l.	<d.l.	<d.l.	<d.l.	<d.l.	<d.l.	<d.l.
Na_2O	<d.l.	<d.l.	<d.l.	<d.l.	<d.l.	<d.l.	<d.l.	0.37	0.10	<d.l.	<d.l.	<d.l.	<d.l.	<d.l.	<d.l.	<d.l.	<d.l.	<d.l.	<d.l.	<d.l.	<d.l.	<d.l.	<d.l.	<d.l.	<d.l.	<d.l.	<d.l.	<d.l.	<d.l.	<d.l.	<d.l.	<d.l.	<d.l.	<d.l.	<d.l.	<d.l.
K_2O	<d.l.	<d.l.	<d.l.	<d.l.	<d.l.	<d.l.	<d.l.	0.30	0.10	<d.l.	<d.l.	<d.l.	<d.l.	<d.l.	<d.l.	<d.l.	<d.l.	<d.l.	<d.l.	<d.l.	<d.l.	<d.l.	<d.l.	<d.l.	<d.l.	<d.l.	<d.l.	<d.l.	<d.l.	<d.l.	<d.l.	<d.l.	<d.l.	<d.l.	<d.l.	<d.l.
Si	5.46	5.78	5.67	5.83	6.05	5.89	5.58	6.57	6.04	5.90	6.26	5.98	5.77	6.48	6.11	5.62	6.11	5.87	5.56	5.82	5.65	5.62	5.84	5.76	5.41	5.87	5.63	5.75	6.22	6.02	5.24	5.96	5.67	5.99	6.56	5.63
Ti	–	–	–	–	–	–	–	0.08	0.03	–	–	–	–	0.19	0.04	–	–	–	–	–	–	–	–	–	–	–	–	–	–	–	–	–	–	–	–	–
Al	5.13	5.41	5.27	4.67	4.99	4.80	3.68	4.86	4.26	4.09	4.80	4.58	3.64	4.82	4.21	4.21	5.03	4.54	4.44	4.74	4.74	4.42	4.76	4.76	4.58	5.34	4.77	4.20	4.50	4.30	4.55	5.17	4.89	4.72	5.26	4.96
Cr	–	–	–	–	–	–	–	0.01	0.01	–	–	–	–	–	–	–	0.04	0.01	–	–	–	–	–	–	–	–	–	–	–	–	–	0.05	–	–	0.03	0.03
Fe'''	–	–	–	–	–	–	–	0.05	0.00	–	–	–	–	–	–	–	0.00	0.00	–	0.08	–	–	–	–	–	0.36	0.06	–	–	–	–	0.09	0.05	–	–	–
Fe''	2.92	5.24	4.13	3.73	4.45	4.14	2.58	3.59	3.10	3.27	4.52	3.85	2.47	2.93	2.69	3.44	4.39	3.87	2.85	3.82	3.42	2.82	3.13	2.93	3.53	4.53	3.99	6.51	6.72	6.63	3.54	5.11	4.20	2.77	4.93	3.45
Mn	–	0.04	0.01	–	0.04	0.01	–	0.05	0.02	–	0.06	0.02	–	–	–	–	0.00	0.00	–	–	–	–	0.05	0.01	–	0.05	0.01	0.11	0.16	0.13	–	0.07	0.05	–	0.04	0.01
Mg	3.68	6.05	4.92	4.71	5.73	5.15	5.92	6.76	6.43	4.95	6.28	5.57	6.48	7.29	6.92	4.95	6.24	5.72	5.67	6.62	6.17	6.39	6.72	6.54	4.46	6.05	5.55	2.78	2.92	2.92	4.06	5.87	5.14	4.41	6.15	5.92
Ca	–	–	–	–	–	–	–	0.40	0.04	–	–	–	–	0.43	0.03	–	0.30	–	–	–	–	–	–	–	–	–	–	–	–	–	–	–	–	–	–	–
Na	–	–	–	–	–	–	–	0.50	0.04	–	–	–	–	–	–	–	–	–	–	–	–	–	–	–	–	–	–	–	–	–	–	–	–	–	–	–
K	–	–	–	–	–	–	–	0.08	0.03	–	–	–	–	–	–	–	–	–	–	–	–	–	–	–	–	–	–	–	–	–	–	–	–	–	–	–
Fe_{tot}	2.92	5.24	4.13	3.73	4.45	4.14	2.58	3.59	3.10	3.27	4.52	3.85	2.47	2.93	2.69	3.44	4.39	3.87	2.85	3.43	3.43	2.82	3.13	2.93	3.53	4.53	4.05	6.51	6.72	6.63	3.54	5.11	4.26	2.77	4.93	3.45
$Al^{(IV)}$	2.25	2.54	2.33	1.95	2.17	2.11	1.43	2.42	1.96	1.70	2.10	2.02	1.52	2.23	1.89	1.87	2.32	2.13	2.16	2.35	2.35	1.86	2.24	2.24	2.21	2.59	2.37	1.70	2.25	1.98	2.00	2.71	2.33	2.01	2.59	2.37
$Al^{(VI)}$	2.80	3.08	2.94	2.54	2.84	2.70	1.96	2.62	2.30	2.39	2.70	2.56	2.00	2.70	2.32	2.34	2.71	2.40	2.28	2.52	2.39	2.52	2.52	2.52	2.12	2.92	2.39	2.14	2.48	2.32	2.20	3.02	2.55	2.59	2.67	2.59
Si/Al	1.02	1.13	1.08	1.17	1.30	1.23	1.15	1.71	1.44	1.24	1.49	1.31	1.08	1.47	1.30	1.21	1.47	1.30	1.19	1.41	1.19	1.21	1.41	1.21	1.14	1.41	1.18	1.22	1.48	1.40	1.13	1.61	1.16	1.14	1.51	1.14
X(Fe)	0.33	0.59	0.46	0.39	0.49	0.45	0.28	0.38	0.33	0.35	0.48	0.41	0.28	0.32	0.28	0.36	0.46	0.40	0.30	0.36	0.36	0.30	0.34	0.31	0.37	0.47	0.42	0.70	0.74	0.70	0.45	0.63	0.45	0.30	0.43	0.37
X(Mg)	0.41	0.67	0.54	0.49	0.60	0.55	0.62	0.71	0.67	0.52	0.66	0.59	0.68	0.76	0.72	0.52	0.65	0.60	0.59	0.70	0.64	0.67	0.70	0.69	0.47	0.63	0.58	0.29	0.30	0.30	0.42	0.61	0.55	0.46	0.64	0.63
T_1**	296	347	313	252	287	277	169	327	253	219	276	263	183	297	242	243	322	281	289	330	316	286	322	299	295	355	320	224	301	256	266	383	313	283	342	320
T_2	254	287	265	225	248	241	170	274	226	203	241	232	179	254	218	219	271	244	249	276	267	247	271	255	253	293	270	206	257	228	234	311	265	245	284	269
T_3	287	315	299	256	284	274	193	297	250	228	271	262	198	299	243	245	304	274	274	302	293	270	294	279	283	322	301	259	309	279	262	352	299	284	307	297
T_4	241	269	250	216	236	230	169	258	217	197	230	222	177	241	210	211	255	232	236	260	252	235	255	242	240	274	254	200	243	218	224	289	250	233	266	254

* Formula units are calculated on the basis of 20 cations;

** T_1 after Cathelineau (1988), T_2 and T_3 after Kranidiotis and McLennan (1987) for low-Al and high-Al environment respectively, T_4 after Kotelnikov et al. (2012)

782 **Table 6.** Microthermometric data of fluid inclusions in quartz and calcite from gold-telluride-
783 bearing assemblages of the Mikheevskoe deposit

Sample, mineral	Incl. type	n	T_h (°C)* (liquid)	T_{solid} (°C)	T_e (°C)	C, wt.% NaCl-equiv.	T_m (CO_2) (°C)	T_h (CO_2) (°C) (mode)	$T_{m(clath)}$ (°C)
M-1-9/15, quartz	L+V+CO_2	4	280 to 320 / 294	–	-29.0 to -26.6/ -27.8	10.2 to 11.0 / 10.6	-57.9 to -57.5 / -58.7	25.4 to 30.0 / 28.2	3.5 to 4.2 / 3.8
	L+V+CO_2	2	295 to 310 / 303	–	-28.8 to -28.0/ -28.4	10.7 to 10.9 / 10.6	–	–	3.7 to 4.0 / 3.9
	L+V+S	3	289 to 318 / 307	280 to 320 / 300	-28.9 to -27.5/ -28.4	10.8 to 11.4 / 11.0	–	–	3.2 to 3.8 / 3.6
	V	3	–	–	–	–	-57.9 to -57.5 / -57.7	26.0 to 28.6 / 27.5	–
M-1/126, quartz	L+V	10	195 to 221 / 211	–	-31.0 to -28.0/ -29.2	3.4 to 5.9/ 4.7	–	–	–
M-7905/190.6, quartz	L+V	6	200 to 220 / 212	–	-31.0 to -28.0/ -29.5	4.9 to 8.3 / 6.5	–	–	–
	L+V+S	3	208 to 218 / 213	200 to 220 / 211	-30.0 to -28.0/ -29.3	6.5 to 8.0 / 7.4	–	–	–
M-1/139, quartz	L+V	8	180 to 217 / 199	–	-62.0 to -57.0/ -59.2	20.4 to 23.0 / 21.7	–	–	–
	L+V+S	3	207	18	-60.2 to -	20.7 to	–	–	–

			to 210 / 208	0 to 217 / 199	57.5/ -58.6	22.0 / 21.4			
M-10405/145, quartz	L+V	6	200 to 230 / 216	–	-62.1 to -57.0/ -60.0	19.6 to 20.9 / 20.4	–	–	–
	L+V+S	3	205 to 220 / 214	200 to 230 / 215	-61.3 to -59.5/ -60.3	19.3 to 20.9 / 20.1	–	–	–
M-5/17, quartz	L+V	11	203 to 221 / 212	–	-36.4 to -30.0 / -33.3	6.3 to 12.3 / 10.3	–	–	–
M-5/17, calcite	L+V	7	172 to 183 / 178	–	-23.4 to -21.8/ -22.7	5.9 to 8.6/ 7.1	–	–	–

* Min to Max / Mean

787 **Table 7.** Comparison of depositional temperatures obtained via chlorite geothermometry and fluid
788 inclusions data

Sample	Precious metals assemblages	Chlorite		Fluid inclusion data		
		chemistry	temperature	temperature measured	temperature P corrected (+30°C)	fluid chemistry
10405/145	Bornite: **Electrum**, **krennerite** (?), **tellurobismuthite,** native Te, Bi sulphide	Si–Al Si/Al to 1.8	177–241/ 210 (12)	200–230/ 215 (9)	230–260/ 245 (9)	Ca–Cl C ≈ 20 wt.%
M-1/139	Chalcopyrite: Krennerite (?), stützite, native Te, galena, **merenskyite, sopcheite**, hessite, tellurobismuthite, coloradoite	Mg–Fe, Si-Al Si/Al =1.2	236–260/ 252 (34)	180-217/ 202 (11) CL	210-247/ 232 (11)	Ca–Cl C ≈ 20 wt.%
M-1/126	Bornite: Stützite, coloradoite, altaite, hessite, native Te	Si–Al? Si/Al =1.2	235–255/ 242 (7)	195-221/ 211(10)	225-251/ 241(10)	Na,Mg–Cl C ≈ 5 wt.%
M-1/142	Bornite: native gold (900), galena	Si-Al Si/Al to1.4	211–255/ 232 (15)	–	–	–
M-52/67.1	Chalcopyrite: Electrum, melonite, altaite	Chl1: Mg–Fe Si/Al =1.1	241–269/ 250 (12)	–	–	–
		Chl2: Si–Al Si/Al =1.2	216–236/ 230 (4)			
M-46/245	Bornite: Electrum, **petzite**, tetradymite, native Te, stützite, hessite	Mg–Fe, Si-Al Si/Al =1.3	197–230/ 222 (7)	–	–	–
M-50/95.2	Chalcopyrite: Tetradymite - kawazulite, hessite, coloradoite	Si–Al, Si/Al = 1.4	169–258/ 225 (18)	–	–	–
M-5/17	Bornite, chalcocite, electrum, hessite, galena	Mg–Fe, Si-Al Si/Al = 1.1	240–274/ 254(18)	203–221/ 212	233–251/ 242	Na,Mg–Cl, C ≈ 10 wt.%
7905/190	Native gold 868–914	Mg–Fe, Si–Al Si/Al = 1.2	224–289/ 250 (12)	200-220/ 212 (9)	230-250/ 242 (9)	Na,Mg–Cl C≈5-8 wt.%
M-1-9/15	Native gold (767-	–	–	280–320/	310–350/	Na,Mg–

	787), tetrahedrite, arsenopyrite			300 (9)	330 (9)	Cl, C ≈ 10 wt.%
M-3-1/16	Electrum 446-522, Ag-tetrahedrite, polybasite	–	–	–	–	–
M-48/137.8	Polybasite, sphalerite, galena, arsenopyrite	Si–Al Si/Al to 1.5	200–243/ 218 (9)	–	–	–
Mikh-7	Electrum, mixture of Te phases	Mg–Fe Si/Al=1.1	240–280 (4)	–	–	–

789
790

- Precious metals (Au, Ag, PGE) minerals at Mikheevskoe are mostly linked to epithermal overprinting
- Precious metal mineralization was deposited from moderately saline fluids at ca. 300 to 200^{o}C
- Variability of precious metal minerals reflect fluctuations of S_2 and/or Te_2 fugacity

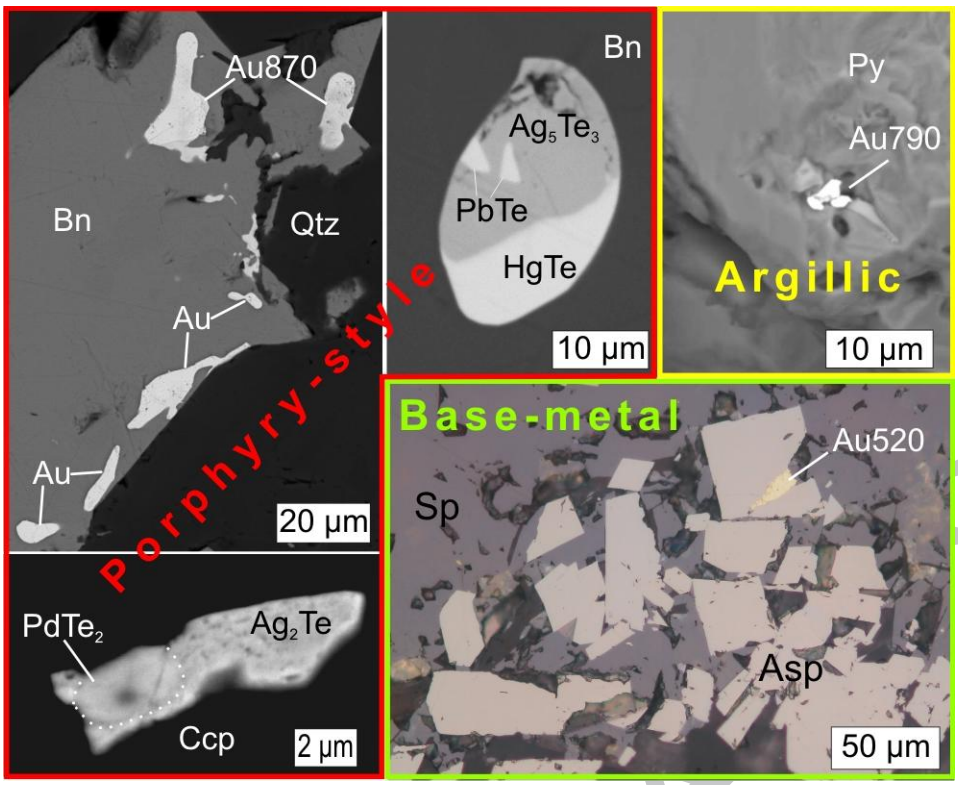

796